Clim. Past Discuss., https://doi.org/10.5194/cp-2017-153
Manuscript under review for journal Clim. Past
Discussion started: 14 December 2017

Climate of the Past Discussions
Open Access
EGU

Oligocene TEX_{86}-derived seawater temperatures from offshore Wilkes Land (East Antarctica)

Keywords:

TEX_{86}

Oligocene

Wilkes Land

sea surface temperature

Antarctic ice sheet

Julian D. Hartman[1], Francesca Sangiorgi[1], Ariadna Salabarnada[2], Francien Peterse[1], Alexander J.P. Houben[3], Stefan Schouten[1,4], Carlota Escutia[2], Peter K. Bijl[1]

[1] Department of Earth Sciences, Utrecht University, Heidelberglaan 2, 3584CS Utrecht, The Netherlands

[2]Instituto Andaluz de Ciencias de la Tierra, CSIC/Universidad de Granada, Avenida de las Palmeras 4, 18100 Armilla, Granada, Spain

[3] Applied Geosciences Team, Netherlands Organisation for applied scientific Research (TNO), Princetonlaan 6, 3584CB Utrecht, The Netherlands

[4]NIOZ Royal Netherlands Institute for Sea Research, and Utrecht University, Landsdiep 4, 1797SZ 't Horntje, Texel, The Netherlands

Correspondence to: Julian D. Hartman (j.d.hartman@uu.nl)

Clim. Past Discuss., https://doi.org/10.5194/cp-2017-153
Manuscript under review for journal Clim. Past
Discussion started: 14 December 2017

Climate of the Past Discussions
Open Access
EGU

Abstract. Today, the temperature of the surface waters near the Antarctic coast is a determining factor in the formation of Antarctic Bottom Water (AABW) through sea-ice production, sea-ice extent, and the extent of the ice shelf. For the Oligocene, deep-sea benthic foraminiferal oxygen isotope ($\delta^{18}O$) reconstructions suggest that the volume of the Antarctic continental ice sheet(s) varied substantially both on million-year and on orbital timescales after its inception in the early Oligocene, and even reached larger than modern-day volumes. Replication of such dynamicity through physical modeling remains problematic, suggesting the existence of complex feedbacks between the cryosphere, the ocean and the atmosphere. To assess the relation between cryosphere, ocean and atmosphere, knowledge of sea surface conditions close to the Antarctic margin is essential. We present a TEX_{86}-based surface water paleotemperature record measured on Oligocene sediments from Integrated Ocean Drilling Program (IODP) Site U1356, offshore Wilkes Land, Antarctica. This record allows us to reconstruct the magnitude of seawater temperature variability and trends on both million-year and on glacial-interglacial timescales. TEX_{86} index values suggest surface temperatures between 10 and 21°C during the Oligocene, which is on the upper end of the few available reconstructions. Sea surface temperature (SST) maxima occur around 30.5 and 25 Ma, irrespective of the calibration equation chosen. Based on glacial-interglacial lithological alternations we have established that SST variability between glacial intervals and their successive interglacials ranged between 1.8 - 3.2°C. As benthic foraminiferal $\delta^{18}O$ data incorporate both an ice-volume and a temperature component, our reconstructed Oligocene temperature variability could have implications for current Oligocene ice-volume estimates. If the long-term ad orbital SST variability is representative of that of the nearby region of deep-water formation, we can assess the impact of this temperature record on the volume and dynamics of the Antarctic ice sheet(s) by comparing it with the $\delta^{18}O$ trends and variability. From this comparison, we argue that a significant portion of the variability and trends contained in long-term $\delta^{18}O$ records can be explained by variability in Southern high-latitude temperature. If indeed a large part of the $\delta^{18}O$ variability is due to large glacial-interglacial bottom-water temperature shifts, the Oligocene Antarctic ice volume was less sensitive to climate change than previously assumed.

Clim. Past Discuss., https://doi.org/10.5194/cp-2017-153
Manuscript under review for journal Clim. Past
Discussion started: 14 December 2017

Climate of the Past Discussions
Open Access
EGU

1 Introduction

Physical paleoclimate models predict that with the current rate of ice volume loss (up to 97.8 Gt/yr, Pritchard et al. 2012) several sectors of the West Antarctic marine-based ice sheet will collapse within the coming few centuries (e.g., Joughin et al. 2014). Observations show that glaciers on East Antarctica are also vulnerable to basal melt through warming of the ocean waters when they are grounded below sea level (Greenbaum et al., 2015; Miles et al., 2016), making the East Antarctic ice sheet (EAIS) not as stable as previously thought (Mcmillan et al., 2014). Recent numerical modelling studies are more in line with the observed ice-sheet volume measurements, because they incorporate positive feedbacks to global warming and more complicated physics into these models (Austermann et al., 2015; Deconto and Pollard, 2016; Fogwill et al., 2014; Golledge et al., 2017; Pollard et al., 2015), and show that sensitivity to global warming is particularly high where the ice sheet is grounded below sea level (Fretwell et al., 2013), such as the Wilkes Land basin.

Both on glacial-interglacial (Parrenin et al., 2013) and longer term Cenozoic timescales (Pagani et al., 2011; Zachos et al., 2008), Antarctic ice-volume changes have been mostly linked to changes in atmospheric CO_2 concentrations (pCO_2, see e.g., Foster & Rohling 2013; Crampton et al. 2016), modulated by astronomical forced changes in solar insolation (e.g., Pälike et al., 2006; Liebrand et al. 2017). Foster & Rohling (2013) compiled past pCO_2 proxy data and associated sea level reconstructions for the last 40 million years (Myr). These data suggest that all ice on West Antarctica and Greenland could be lost under current and near future atmospheric CO_2 conditions (400-450 ppmv) in equilibrium state. Projections of pCO_2 for the future emission scenarios of the latest IPCC Report (2014) show a range between 500 and 1000 ppmv for the year 2100, which could imply additional loss of East Antarctic ice-sheet volume. This range in atmospheric pCO_2 is similar to that reconstructed for the Oligocene epoch (e.g., Zhang et al. 2013), highlighting the importance to constrain near-field sea surface temperatures (SSTs) from the Oligocene Antarctic margin.

EAIS volume changes have been suggested for the Oligocene based on a number of deep-sea $\delta^{18}O$ records (Liebrand et al., 2017; Pekar et al., 2006; Pekar and Christie-Blick, 2008), which reflect a combination of bottom-water temperature and ice volume. These records show long-term (1-3 Myr) trends: a shift towards lighter $\delta^{18}O$ after the Oi-1 event and a steady increase towards 27 Ma, then a decrease to 24 Ma and a final increase leading to the Mi-1 event (Beddow et al., 2016; Cramer et al., 2009; Liebrand et al., 2016; Zachos, 2001). The high-resolution records show that these trends are punctuated by strong but transient glaciation events (Hauptvogel et al., 2017; Liebrand et al., 2017, 2016; Pälike et al., 2006). These glaciations are paced by periods of strong 110-kyr eccentricity fluctuations of up to 1‰ (Liebrand et al., 2017, 2016, 2011). Either these $\delta^{18}O$ fluctuations are mostly resulting from the waxing and waning of the EAIS, in which case the ice sheet must have been highly dynamic, or they reflect large changes in deep-sea temperature, in which case large SST fluctuations in the region of deep-water formation must be expected. Considering the former, fluctuations between 50% and 125% of the present-day EAIS have been suggested (DeConto et al., 2008; Pekar et al., 2006; Pekar and Christie-Blick, 2008), but this amount of variability has not yet been entirely reproduced by numerical modeling studies (DeConto et al., 2008; Gasson et al., 2016; Pollard et al., 2015). Considering the latter, several studies have suggested that during the Oligocene the southern high latitudes were the prevalent source for cold deep-water formation (Katz et al. 2011; Goldner et al. 2014; Borelli

& Katz 2015). Hence, temperature records from the southern high-latitudes, particularly those capturing temperature changes on million-year as well as orbital timescales, may provide information on the relative contribution of deep-sea temperature variability in the $\delta^{18}O$ records, and as such should reflect the sensitivity of Antarctic ice sheets to CO_2 concentrations. Assuming that the deep-sea temperature trend captured in the Oligocene $\delta^{18}O$ records is related to surface water temperature in the Southern Ocean similarly to today (Baines, 2009; Jacobs, 1991), ice-proximal SST would potentially gauge the Oligocene deep-sea temperature variability. Only few early Oligocene SST estimates are available for the Southern Ocean (Petersen and Schrag, 2015; Plancq et al., 2014). Obstacles for reconstructing Oligocene SST in the Southern Ocean are the paucity of stratigraphically well-calibrated sedimentary archives, as well as suitable indicator fossils/compounds within these sediments that can be used to reconstruct SST. In this study we use the ratio between several glycerol dialkyl glycerol tetraethers (GDGTs), the TEX_{86} SST proxy. These resistant organic compounds are often the only fossil remains that preserve, because biogenic carbonate and silica dissolve under the corrosive bottom-water conditions of the high-latitude Southern Ocean.

In 2010, the Integrated Ocean Drilling Program (IODP) drilled a sedimentary archive at the boundary of the continental rise and the abyssal plain offshore Wilkes Land that does contain a well-dated and complete Oligocene sequence: IODP Site U1356 (Fig. 1). We here reconstruct the first SST record from high Southern Ocean latitude based on TEX_{86} covering almost the entire Oligocene and compare it with the few existing early Oligocene SWT data from other high latitude Southern Ocean sites (ODP Sites 511 and 689) and with deep-water $\delta^{18}O$ records from lower latitudes. Although the TEX_{86}-SST relation shows scatter in the low-temperature (<5°C) domain (Kim et al., 2010, 2008), more regional modern-analogue calibration methods exist today to overcome some of the scatter (Tierney and Tingley, 2015, 2014). Still, TEX_{86} is known to overestimate temperatures at high latitudes due to multiple possible biases (Ho et al., 2014; Ho and Laepple, 2016; Schouten et al., 2013). However, there is general consensus that TEX_{86} is able to capture decadal and longer-term temperature trends (Ho and Laepple, 2016; Richey and Tierney, 2016), which is why our main focus lies on relative SST changes.

The Wilkes Land region is one of the regions of East Antarctica sensitive to warming, because most of the bedrock lies below sea level today (Fretwell et al., 2013; Golledge et al., 2017) and Site U1356 may therefore have recorded past dynamics of the East Antarctic ice sheet. However, during the Oligocene the ice sheet was likely not marine-based (Wilson et al., 2012). Still, detailed lithological logging of the section allows the distinction of glacial and interglacial deposits (Salabarnada et al., submitted this volume). This enables us to assess long-term evolution of SWT in proximity of the ice-sheet as well as the temperature differences between glacials and interglacials on orbital time scales, which have implications on the dynamics of the Oligocene Antarctic ice-sheet and its sensitivity to climate change.

2 Materials & Methods

2.1 Site description

Integrated Ocean Drilling Program (IODP) Expedition 318 Site U1356 was drilled about 300 kilometers off the Wilkes Land coast at the boundary between the continental rise and the abyssal plain at a water depth of 3992 m

Clim. Past Discuss., https://doi.org/10.5194/cp-2017-153
Manuscript under review for journal Clim. Past
Discussion started: 14 December 2017

(Escutia et al. 2011, see Fig. 1). Today, this site is positioned south of the Antarctic Polar Front (PF) and is thus under the influence of by Antarctic Bottom Waters (AABW), Lower Component Deep Water (LCDW), and Antarctic Surface Water (AASW).

2.2 Sedimentology

At present, IODP Site U1356 receives sediments transported from the shelf and the slope as well as *in situ* pelagic component. Detailed logging of the sediments recovered in Hole U1356A has revealed that the Oligocene sedimentary record (between 431.74 and 894.80 meters below sea floor) consists mostly of alternations of laminated and bioturbated sediments, mass transport deposits (MTDs), and carbonate beds (Salabarnada et al., submitted this volume) (Fig. 2). Samples from the mass-waste beds seem to contain the largest contribution of reworked older material transported from the continental shelf (Bijl et al., submitted this volume), while in the other lithologies, this component is much more reduced or absent altogether.

Between 593.4 and 795.1 meters below sea floor, clear alternations between greenish, carbonate-poor laminated and grey bioturbated deposits with some carbonate-rich bioturbated deposit. These deposits have been interpreted as contourite deposits recording glacial-interglacial environmental variability (Salabarnada et al., submitted this volume). Above 600 mbsf these alternations are less clear, and the sediments mostly consist of MTDs (Fig. 2). However, between the MTDs greenish or grey laminated deposits and greenish or grey bioturbated deposits are preserved. Near the bottom of Unit III (around 433 mbsf) a different depositional setting is represented with alternations between pelagic clays and ripple cross-laminated sandstone beds (Escutia et al., 2011). Samples analyzed for TEX_{86} are chosen from all the 7 different lithologies (Fig. 2). In particular the carbonate-poor laminated and (carbonate-rich) bioturbated deposits have been sampled, so we can test whether the glacial-interglacial variability inferred from the lithology is reflected in our TEX_{86} data.

2.3 Oceanographic setting

The details of the Oligocene Southern Ocean oceanographyare not fully understood. Studies suggest most Southern Ocean surface and deep water masses were already in place by the Eocene-Oligocene Boundary times (Katz et al., 2011). Neodymium isotopes on opposite sides of Tasmania suggest that an eastward flowing deep-water current was present since 30 Ma (Scher et al., 2015). A westward flowing Antarctic Circumpolar Counter Current (ACCC) was already established during the late Eocene (49 Ma; Bijl et al. 2013) (Fig. 1). Opening of the Tasmanian gateway also allowed the proto-Leeuwin current flowing along southern Australia continue eastward (Carter et al., 2004; Stickley et al., 2004) (Fig. 1). Despite these reconstructions, numerical modeling studies showed that both Australia and South America were substantially closer to Antarctica (Fig. 1) than today, which must have limited throughflow of the Antarctic Circumpolar Current (ACC) during the Oligocene (Hill et al., 2013). Moreover, tectonic reconstructions and stratigraphy of formations on Tierra del Fuego suggest Drake Passage underwent temporal closure from 29 Ma onwards following open conditions in the middle and late Eocene (Lagabrielle et al., 2009). If throughflow at Drake Passage was indeed limited in the Oligocene (Lagabrielle et al., 2009), the model study of Hill

et al. (2013) suggests that the ACCC was more dominant than the ACC. Antarctica itself was positioned more eastward during the Oligocene relative to today (foremost due to true polar wander; van Hinsbergen et al., 2015), leading to a relative northward position of U1356 during the Oligocene compared to today. Because of this, bottom-water formation did likely not occur at U1356A. Instead, bottom-water formation is expected in more southerly positioned shallow basins, and where glaciers extended onto the Antarctic shelf, such as the nearby Ross Sea (Sorlien et al., 2007).

2.4 Stratigraphic age model U1356

Oligocene sediments were recovered in the section from 894.68 mbsf (first occurrence (FO) *Malvinia escutiana*) to 432.64 mbsf (base of chron C6Cn.2n) at IODP Hole U1356A. The shipboard age model (Tauxe et al., 2012) was based on biostratigraphy with magnetostratigraphic tie points and chronostratigraphically calibrated to the Geologic Timescale of 2004 (Gradstein et al., 2004). We follow Bijl et al. (accepted), who recalibrated the existing age tie points to the Geologic Timescale of 2012 (GTS2012, Gradstein et al., 2012). The FO of *Malvinia escutiana* (894.68 mbsf; 33.5 Ma; Houben et al., 2011) and the last occurrence (LO) of *Reticulofenestra bisecta* (431.99 mbsf; 22.97 Ma) and the paleomagnetic tie points were used to convert the data to the time domain (see Fig. 4). For the Oligocene-Miocene Boundary, we also follow Bijl et al. (submitted) who infer a hiatus spanning ~22.5-17.0 Ma between Cores 44R and 45R (~421 mbsf). It is unknown whether hiatuses exist within the Oligocene record, but this is likely considering the presence of MTDs (Salabarnada et al., submitted this volume; Fig. S1). In addition, the poor core recovery in some intervals dictates caution in making detailed stratigraphic comparisons with other records.

2.5 Glycerol dialkyl glycerol tetraether extraction and analysis

A total of 129 samples from the Oligocene part of the sedimentary record (Table S1) have been processed for the analysis of glycerol dialkyl glycerol tetraethers (GDGTs) used for TEX_{86}. Sample spacing varies due to variability in core recovery and GDGT preservation. Furthermore, sampling of contorted bedding was avoided. Sample processing involved manual powdering of freeze-dried sediments after which lipids were extracted through accelerated solvent extraction (ASE; with dichloromethane (DCM)/methanol (MeOH) mixture, 9:1 v/v, at 100°C and 7.6 x 10^6 Pa). The lipid extract was separated using Al_2O_3 column chromatography and hexane/DCM (9:1, v/v), hexane/DCM (1:1, v/v) and DCM/MeOH (1:1, v/v) for separating apolar, ketone and polar fractions, respectively. Then, 99 ng of C_{46} internal standard was added to the polar fraction, containing the GDGTs, for quantification purposes (cf. Huguet et al., 2006). The polar fraction of each sample was dried under N_2, dissolved in hexane/isopropanol (99:1, v/v) and filtered through a 0.45-µm 4-mm-diameter polytetrafluorethylene filter. After that the dissolved polar fractions were injected and analyzed by high performance liquid chromatography/mass spectrometry (HPLC/MS) at Utrecht University. Most samples were analyzed following HPLC/MS settings in Schouten et al. (2007), while some samples (see Table S1) were analyzed by ultra-high performance liquid chromatography/mass spectrometry (UHPLC/MS) according to the method described by (Hopmans et al., 2016). Only a minor difference between TEX_{86} index values generated by the different methods was recorded by Hopmans

Clim. Past Discuss., https://doi.org/10.5194/cp-2017-153
Manuscript under review for journal Clim. Past
Discussion started: 14 December 2017

et al. (2016) (on average 0.005 TEX_{86} units). Reruns of 5 samples with the new method show an average difference between the two methods of 0.011 TEX_{86} units (see Table S2), which translates to a 0.6°C temperature difference based on TEX_{86}^{H} of (Kim et al., 2010) and lies well within the calibration error of 2.5°C. GDGT peaks in the (U)HPLC chromatograms were integrated using Chemstation software. Sixteen of the 129 samples had too low concentrations of GDGTs to obtain a reliable TEX_{86} value and have been discarded. We have used the branched and isoprenoid tetraether (BIT) index (Hopmans et al., 2004) to verify the relative contribution of terrestrial GDGTs in our samples, compared to marine GDGTs. As isoprenoid GDGTs (isoGDGTs), used for the TEX_{86} proxy are also produced in terrestrial soils, albeit in minor amounts, they can alter the marine signal when there is a large contribution of soil organic matter to marine sediments. This contribution can be identified by determining the relative amount of branched GDGTs (brGDGTs), which are primarily soil-derived (Weijers et al., 2006), to that of the isoGDGT crenarchaeol (Hopmans et al., 2004). Samples with BIT index values above 0.3 indicate that the TEX_{86}-based temperature may be affected by a contribution of soil-derived isoGDGTs and thus should be discarded (cf. Weijers et al. 2006). However, a high BIT value could also result from production of brGDGTs in marine sediments and the water column (Peterse et al., 2009; Sinninghe Damsté, 2016). Still the composition of the brGDGTs can be used to distinguish between marine and soil-derived GDGT input, in particular by using the $\#ring_{tetra}$ index (Sinninghe Damsté, 2016). We have applied this index on samples analyzed by UHPLC/MS to see if TEX_{86} values are reliable despite high BIT index values. In addition, we calculated the Methane Index (MI) (Zhang et al., 2011), GDGT-0/crenarchaeol (Blaga et al., 2009; Sinninghe Damste et al., 2009), GDGT-2/crenarchaeol ratios (Weijers et al., 2011), and Ring Index (Zhang et al., 2016) to check for input of methanogenic or methanotrophic archaea, or any other non-temperature related biases to TEX_{86}.

2.6 TEX_{86} calibrations

The TEX_{86} proxy is based on the distribution of isoGDGTs preserved in sediments (Schouten et al., 2002). In marine sediments these lipids originate from cell membranes of marine Thaumarchaeota, which are one of the dominant prokaryotes in today's ocean and occur throughout the entire water column (e.g. Karner et al. 2001; Church et al. 2003; Church et al. 2010). Applying TEX_{86} in polar oceans has been challenged by the observation that high scatter in the cold end of the core top dataset for TEX_{86} is present (Ho et al., 2014; Kim et al., 2010). Kim et al. (2010) improved the calibration for the polar ocean, by proposing the TEX_{86}^{L}. In addition, Ho et al. (2014) showed that the scatter is more caused by regional TEX_{86} variability in the Arctic Ocean rather than by the Southern Ocean core top. In turn, Southern Ocean TEX_{86}^{L} values appear to be biased towards higher temperatures and correlate best with annual summer temperatures (Ho et al., 2014) due to relatively high amounts of GDGT-3 versus GDGT-2. In addition, it has been shown that the distribution of GDGTs and also the GDGT-2/GDGT-3 ratio in the water column is strongly influenced by the abundance of the 'shallow' and 'deep water' Thaumarchaeotal clades (Taylor et al., 2013; Villanueva et al., 2015), of which the deep community is strongly affected by changes in ammonia or oxygen concentrations (Basse et al., 2014; Villanueva et al., 2015). Close to the Antarctic margin, the abundance of 'shallow' versus 'deep water' Thaumarchaeotal communities at deep water sites, like Site U1356, could be affected by the presence of sea ice and the relative influence of (proto-)Component Deep Water upwelling. Therefore, Site

U1356 might have been susceptible to Thaumarchaeotal community changes, which affect the GDGT-2/GDGT-3 ratio. As GDGT-3 is not included in the nominator of TEX_{86}^{L}, changes in the GDGT-2/GDGT-3 ratio will affect TEX_{86}^{L}-based SST reconstructions to a large extent. For this reason, TEX_{86}^{L}-based calibrations are not the focus of our study, but have been included together with all existing $TEX_{86}^{(H)}$ calibrations as a supplementary figure (Figure S1).

It has been shown that highest GDGT fluxes are closely linked to highest organic matter, opal (diatom frustules) and lithogenic particle fluxes (Mollenhauer et al., 2015; Yamamoto et al., 2012). A lack of production of sinking particles that can incorporate GDGTs formed in deeper waters prohibits that surface-sediment TEX_{86} values are biased towards deep-water temperatures (Basse et al., 2014; Mollenhauer et al., 2015; Yamamoto et al., 2012). Still, particular environmental settings (e.g., upwelling regions, regions with oxygen-depleted deep waters, fresh-water surface waters) might favor the transport of a subsurface temperature signal to the sediments (Kim et al., 2012a, 2012b; Lopes dos Santos et al., 2010; Mollenhauer et al., 2015). Also for polar oceans it has been suggested that reconstructed temperatures reflect subsurface temperatures, as today Thaumarchaeota are virtually absent in the upper 0-45 m of Antarctic low-salinity surface waters (Kalanetra et al., 2009). Surface water conditions over Site U1356 during the Oligocene were much like present-day regions just south of the Subtropical Front (STF) (see Fig. 1) (Bijl et al., submitted this volume). Thus, there is no reason to believe that TEX_{86} values are influenced by subsurface temperatures as a result of low-salinity surface waters due to sea ice melt. Therefore, subsurface temperature TEX_{86} calibrations are not discussed. However, they have been included in Figure S1.

Based on the above, we here use the linear SST calibration in Kim et al. (2010). Despite the inclusion of Arctic surface sediment samples with deviating TEX_{86}-SST relations, this calibration ($SST = 81.5*TEX_{86} - 26.6$ with a calibration error of ±5.2°C) has been shown to plot onto the annual mean sea surface temperatures of the World Ocean Atlas 2009 (WOA2009; Locarnini et al. 2010) for the TEX_{86} values obtained from surface samples in the Pacific sector of the Southern Ocean (Ho et al., 2014). However, this calibration is likely to be influenced by regional differences in water depth, oceanographic setting and archaeal communities (Kim et al., 2016; Tierney and Tingley, 2014; Trommer et al., 2009; Villanueva et al., 2015). To evaluate the regional variability of the TEX_{86}-SST relation, we have compared the linear TEX_{86} calibration of Kim et al. (2010) with the calibration model of Tierney & Tingley (2014; 2015). The latter calibration is based on a Bayesian spatially varying regression model (BAYSPAR), which infers a best estimate for intersection and slope of the calibration based on an assembly of 20° by 20° spatial grid boxes that statistically fit best with a prior estimate of average SST for our SST record. The prior for site U1356 is obtained from recent clumped isotope measurements (Δ_{47}) on planktonic foraminifers from Maud Rise (ODP Site 689) (Petersen and Schrag, 2015), which show early Oligocene temperatures of 12°C.

To get an estimate for the long-term average SWT trends and confidence levels a Local polynomial regression model (LOESS) has been applied using R, which is based on the local regression model *cloess* of Cleveland et al. (1992). This method of estimating the long-term average trend is preferred over a running average, because it accounts for the variable sample resolution. For the parameter *span*, which controls the degree of smoothing a value was automatically selected through generalized cross-validation (R-package fANCOVA; Wang 2010).

Clim. Past Discuss., https://doi.org/10.5194/cp-2017-153
Manuscript under review for journal Clim. Past
Discussion started: 14 December 2017

3 Results

3.1 Discarding potentially biased TEX_{86} values

Of the 129 samples analyzed, 113 contained sufficient GDGTs to obtain a TEX_{86} value. However, only 69 of these 113 TEX_{86} values could be used for SST reconstruction as discussed below.

Twenty-eight samples were taken within distorted beddings, likely the distal reaches of MTDs originating from the slope or outer shelf of the Wilkes Land Margin (lithological Units IV, VI, VIII and IX) (Escutia et al., 2011). Hence, samples from these beds may not reflect *in situ* material exclusively. In addition, dinoflagellate cyst assemblages show a high degree of reworked Eocene species below 880.08 mbsf (Houben et al., 2013). To avoid potential bias due to allochtonous input and reworking of older sediments, all samples from MTDs and from below 880.08 mbsf are also excluded from the SST reconstructions. In addition, the clast-bearing deposits of Unit IV and decimeter-thick granule-rich interbeds of Unit VIII (Fig. 2) are interpreted as ice-rafted debris (IRD) deposits (Escutia et al., 2011), and thus indicate the presence of ice bergs above the site during deposition of these intervals.

A contribution of terrestrial isoGDGTs can also bias the marine pelagic TEX_{86} signal, and can be verified by the BIT index (Hopmans et al., 2004; Weijers et al., 2006). In nine samples – none of which were derived from mass waste or IRD deposits – the BIT index value was >0.3, which indicates that the reconstructed TEX_{86}-temperatures are likely affected by a contribution of soil-derived isoGDGTs (Weijers et al., 2006; Hopmans et al. 2004). For those samples which were analyzed by UHPLC/MS, the composition of brGDGTs was analyzed to see if high BIT index values are the result of high marine brGDGT input, but none of these samples had $\#rings_{tetra}$ above 0.7 (Sinninghe Damsté, 2016) meaning that a significant portion of the brGDGTs was likely soil-derived. All of these samples are therefore discarded.

Furthermore, the TEX_{86} signal may be influenced by a potential input of isoGDGTs from methanogenic archaea. Since methanogenic Euryarchaeota are known to produce GDGT-0 (Koga et al., 1998), but not crenarchaeol such a contribution may be recognized by GDGT-0/crenarchaeol values >2, as well as values >0.3 for the Methane Index (MI) (Blaga et al., 2009; Sinninghe Damsté et al., 2009; Weijers et al., 2011; Zhang et al., 2011). Thirteen samples have GDGT-0/crenarchaeol ratios > 2 and/or too high Methane Index values (Zhang et al., 2011). Eight of these also had too high BIT index values, and thus an additional five were discarded. No samples had GDGT-2/crenarchaeol ratios > 0.4, indicating no GDGT input from methanotrophs (Weijers et al., 2011). As a final exercise, the Ring Index (|ΔRI|) has been calculated for our dataset to identify all other non-temperature related influences on TEX_{86} (Zhang et al., 2016). Using |ΔRI|>0.6 as a cutoff, two more samples were discarded. All GDGT data and TEX_{86} values, including that of the discarded samples, are presented in the supplementary material (Figure S2, Table S1). Table S1 also shows the GDGT-2/GDGT-3 ratios, which show a large variation among the non-discarded samples. This justifies our choice for a TEX_{86}-based SST reconstruction over a TEX_{86}^{L}-based SST reconstruction as large shifts in the GDGT-2/GDGT-3 ratio will affect the reconstructed SST trends, particularly below a value of 4 (Taylor et al., 2013).

3.2 Relation between TEX_{86} values and lithology

Clim. Past Discuss., https://doi.org/10.5194/cp-2017-153
Manuscript under review for journal Clim. Past
Discussion started: 14 December 2017

After excluding samples with potentially biased TEX_{86} values, the remaining, assumed *in situ* pelagic temperature signal could be interpreted. We note that the short-term variability in the record seems to be strongly linked to the lithology (see Fig. 2); Samples obtained from the greenish laminated, carbonate-poor (glacial) facies produce statistically significant (p-value<0.002 of t-test) lower TEX_{86} values than values obtained from the grey carbonate-rich bioturbated (interglacial) facies. Between 600 and 879 mbsf, TEX_{86} values are on average 0.51 and 0.56 for the glacial (laminated) and interglacial (bioturbated) lithologies, respectively. Also in Units III and IV the bioturbated beds are associated with relatively higher TEX_{86} values compared to the values obtained from the (cross-)laminated beds, although the difference between intervals in those Units is slightly less.

3.3 Oligocene long-term sea surface temperature trend

Based on the linear temperature calibration of Kim et al. (2010) (black curve in Fig. 3A), our TEX_{86} index values give an average SST of 16.3 (±5.2°C calibration error) for the Oligocene. Maximum and minimum temperatures are 25.1°C±5.2°C and 8.3°C±5.2°C, respectively. For 90% of the samples reconstructed temperatures fall between 10.5±5.2°C and 20.8±5.2°C (Fig. 3A). Apart from the highest temperatures around 25.5 Ma, high SSTs are also reconstructed for the period around 30.5 Ma (up to 22.6±5.2°C), whereas the interval after 23.5 Ma displays lower temperatures. SST variability increases significantly (p-value<0.001 in F-test) after 26.5 Ma (see Fig. 3B). Before 26.5 Ma, the variation in the record has a double standard deviation (2σ) of 3.6°C, while the 2σ is 6.8°C after 26.5 Ma. We note a strong (9.5°C) SST drop at the lower boundary of what is interpreted as chron C6Cn.2n (23.03 Ma) (see Fig. 2 and 4); at the stratigraphic position of maximum $\delta^{18}O$ values related to Mi-1 in the deep-sea records (Beddow et al., 2016; Liebrand et al., 2011; Pälike et al., 2006). Unfortunately, due to core recovery issues, limited high-resolution biostratigraphic control and the nature of the sediments, the age model is generally too crude to identify some of the other known transient temperature drops in our record (~30 Ma, ~24 Ma) to Oligocene glaciation-related Oi-events (Fig. 4).

The BAYSPAR approach (Tierney & Tingley 2014; 2015) selects only those TEX_{86} values from the calibration set of Kim et al. (2010) that are relevant for a study site, thereby generating a more regional calibration. The SST curve for U1356 based on the BAYSPAR model shows the same trend as the SST record generated with the linear calibration, but is consistently offset by 1.0±0.7°C , and has a smaller calibration error (3.5°C) (red curve in Fig. 3A). This offset and the smaller calibration error result primarily from the fact that BAYSPAR-calibration does not take the polar TEX_{86} core-top values into account. Instead, it bases its calibration mostly on the modern 30-50° northern and southern latitudinal bands (see map in Fig. 3). Nevertheless, the offset lies well within the ±5.2°C calibration error of the transfer function from Kim et al. (2010), as well as within the standard error of about 3.5°C for the BAYSPAR calibration. In summary, SSTs from the BAYSPAR calibration are very similar to the SSTs derived with the linear calibration, in absolute values, long-term trends, as well as amplitude of variability.

Clim. Past Discuss., https://doi.org/10.5194/cp-2017-153
Manuscript under review for journal Clim. Past
Discussion started: 14 December 2017

4 Discussion

4.1 Oligocene Southern Ocean sea surface temperature estimates

Our TEX_{86}-derived Southern Ocean SWT record is the first that covers almost the entire Oligocene. Absolute temperature values are relatively high considering the high-latitude position of Site U1356. However, considering that TEX_{86}-based reconstructed SSTs obtained from interpreted glacial lithologies are generally lower than those obtained from interglacial lithologies (Fig. 4), strongly supports that our TEX_{86} record is reflecting temperature. Several lines of evidence seem to support the relatively high Oligocene temperatures reconstructed for Site U1356. Dinoflagellate cyst assemblages from the same site (Bijl et al., submitted this volume) mostly contain taxa related to those found between the Polar (PF) and the Subtropical Front (STF), where mean annual sea surface temperature is between 8 and 16°C (Prebble et al. 2013), which is on the low end of our reconstructed SSTs. Furthermore, the abundance of *in situ* pollen of temperate vegetation in these sediments (Strother et al., 2017), which most likely derive from the Antarctic coastline, also suggests a relatively mild climate. Finally, the abundance of pelagic carbonaceous facies in some of the interglacial intervals of these high-latitude is interpreted to occur under the influence of northern-sourced surface waters at Site U1356 (Salabarnada et al., submitted this volume).

TEX_{86}-derived SSTs for IODP Site U1356 are generally higher than those reconstructed with other proxies in other high-latitude Southern-Ocean sites during the early Oligocene (between ~ 34 and ~ 32 Ma; Fig. 3A). However, the ~12°C (standard error: ±1.1-3.5°C) based on clumped isotopes for Site 689 is derived from thermocline-dwelling foraminifera, whereas the temperature of the surface waters were likely higher than that at the thermocline (Petersen and Schrag, 2015). In addition, when the newest calibration for clumped isotope data is applied (Kelson et al., 2017) also higher temperature estimates, 12.8-14.5°C, are obtained. Temperatures between 6 to 10°C have been obtained from ODP Site 511 (see Fig. 1) based on $U^{K'}_{37}$ (Plancq et al., 2014) and TEX_{86} values (Liu et al., 2009), the latter recalculated with the linear calibration of Kim et al. (2010) used here (Fig. 3A). The influence of the cold Antarctic-derived surface current prevailing at Site 511 (Bijl et al., 2011; Douglas et al., 2014) (Fig. 1) might be the reason of these colder estimates. Meanwhile, similar to the Eocene, Site U1356 probably represents one of the warmest regions around Antarctica during the early Oligocene (Pross et al., 2012), situated at a relatively northerly latitude (Hinsbergen et al., 2015) and still under influence of relatively warm proto-Leeuwin current (PLC, Fig. 1) (Bijl et al. 2011; submitted this volume).

Biota-based temperature reconstructions at such high latitudes can be skewed towards summer, as has also been suggested for Site 689 and Site 511 (Petersen and Schrag, 2015; Plancq et al., 2014). An important reason for this could be the light limitation at high latitudes during winter (e.g., Spilling et al. 2015), which is unfavorable for the growth and bloom of phytoplankton, and organisms feeding on phytoplankton. Indeed, isoGDGTs likely require pelleting to sink effectively through the water column to the ocean floor (e.g., Schouten et al. 2013). As phytoplankton blooms mostly occur during Antarctic summer/autumn, as do their predators, the copepods (Schnack-Schiel, 2001), we expect the highest isoGDGT fluxes to the sediment during the summer in the Southern Ocean, despite their primary production during a different season (Church et al., 2003; Murray et al., 1998; Richey and Tierney, 2016; Rodrigo-Gámiz et al., 2015).

Clim. Past Discuss., https://doi.org/10.5194/cp-2017-153
Manuscript under review for journal Clim. Past
Discussion started: 14 December 2017

4.2 Long-term Oligocene sea surface temperature variability

We aim to use our TEX_{86}-based SST record to distinguish between the temperature and the ice-sheet signal captured in the global $\delta^{18}O$ trend. Due to the relatively low sample resolution and poor age model of our record in comparison to the $\delta^{18}O$ records (Hauptvogel et al., 2017; Liebrand et al., 2017, 2016; Pälike et al., 2006), we will here focus on the long-term temperature trends. We can use the glacial-interglacial alternations in the lithology, which cover the period between 32 and 25 Ma, to differentiate between glacial and interglacial reconstructed SSTs (see Fig. 2). Separating glacial and interglacial signals allows us to interpret the long-term SST trend, as this removes a potential sampling bias towards more glacial or more interglacial deposits. To obtain both long-term glacial and interglacial SST trends, LOESS curves are plotted through SST estimates from the glacial and interglacial subsets. The LOESS curves through the glacial and interglacial data show similar trends (Fig. 4): SSTs increase from the earliest Oligocene towards 30.5 Ma, followed by a cooling trend until around 28-27 Ma, followed by warming towards a long-term optimum around 26 Ma, and then cooling towards the Oligocene-Miocene transition at 23 Ma. The recorded post-Oi-1 SST warming coincides with the disappearance of IRD (Escutia et al., 2011) and sea-ice related dinoflagellate cysts (Houben et al., 2013) in the same record (Fig. 4). The second temperature optimum between 26.5 and 25 Ma is characterized by the influx of the dinocyst genus *Nematosphaeropsis* (Bijl et al., submitted this volume). This seems to indicate a strong influence of northern-sourced surface waters (PLC, Fig. 1) at Site U1356 , as this species is currently associated with the Subtropical Front and mean annual temperatures above 11°C (Esper and Zonneveld, 2007; Marret and De Vernal, 1997; Prebble et al., 2013).

Site U1356 probably was not in the region of deep-water formation, given it probably was the warmest region around Antarctica (Pross et al., 2012) likely also in the Oligocene. Nevertheless, because Antarctic Circumpolar Countercurrent (ACCC) (Bijl et al., 2013) and bottom-water formation along the associated Antarctic Slope Front (ASF) were likely established near U1356 in the early Oligocene (Scher et al., 2015), we expect that bottom-water formation was under the influence of the same long-term (million-year) climatic trends recorded in the SST reconstruction of Site U1356. In turn, Southern Ocean surface-water temperatures were likely relayed to the deep-ocean. In fact, Southern Ocean sourced deep waters may have reached all the way to the north Pacific during the Oligocene (Borelli & Katz 2015). This suggests that deep-sea benthic foraminiferal $\delta^{18}O$ records have incorporated both a temperature and ice-volume signal present in the Antarctic-derived deep-waters. Indeed, the only bottom-water temperature record available for the Oligocene, which is based on Mg/Ca ratios of benthic foraminifera from Site 1218 (equatorial Pacific) (Lear et al. 2004; Fig. 4), shows a long-term warming between 27 and 25 Ma, similar to our SST record. Notably, Mg/Ca-based reconstructed bottom-water temperatures at Site 1218 are much lower than reconstructed SSTs from Site U1356: 3.7°C on average (Lear et al. 2004; Fig. 4). Likely, this difference results from the fact that bottom water forms at higher latitudes in the subsurface in winter (Jacobs, 1991), while our TEX_{86}–based SST record likely reflects summer temperatures. The temperature rise before 30.5 Ma and the temperature decrease after 25 Ma in our TEX_{86}-based SST record cannot be recognized in the bottom-water temperature record of Site 1218. Uncertainties about Mg/Ca ratio of the seawater and the influence of a changing carbonate ion saturation state of the deep waters at Site 1218 (Elderfield et al., 2006; Lear et al., 2010), as well as a

lack of a high-resolution age model of our record and low sample resolution compromise a detailed comparison between the two records.

With the here reconstructed SST record, we can now evaluate what part of the long-term $\delta^{18}O$ trend can be explained by high-latitude SST changes. We compare our SST record to the high-resolution Oligocene deep-sea $\delta^{18}O$ record from the equatorial Pacific (Site 1218; Pälike et al. 2006), which is the only high-resolution $\delta^{18}O$ record that covers the entire Oligocene. To enable direct comparison, we have resampled the glacial (values above average $\delta^{18}O$) and interglacial (values below average $\delta^{18}O$) $\delta^{18}O$ trends at Site 1218 following the sample resolution of U1356 (Fig. 4). Part of the long-term benthic $\delta^{18}O$ trend from Site 1218 is reflected in our TEX_{86}-based SST record (Fig. 4): both glacial and interglacial SST LOESS curves show a decreasing trend towards 27 Ma co-occurring with the long-term 0.6‰ $\delta^{18}O$ increase observed between 32 and 27 Ma. The subsequent decrease in $\delta^{18}O$ is also matched by an increase in the long-term interglacial and glacial SST curves. This means that in this part of the record, long-term bottom-water temperature changes could account for part of the long-term $\delta^{18}O$ trends. However, other parts of the record show a mismatch between the long-term SST trend and the long-term $\delta^{18}O$ trend. For example, our reconstructed SST record shows increasing temperatures between 33 and 30.5 Ma, while $\delta^{18}O$ values decrease only between 33.5 and 32 Ma. Furthermore, reconstructed SSTs start decreasing after 25 Ma, while $\delta^{18}O$ values start increasing only after 24 Ma. However, low sampling resolution and uncertainties in the age model might account for these mismatches.

The striking similarity between the SST and $\delta^{18}O$ long-term trends in the interval between 30.5 and 25 Ma, despite reconstructed SSTs at Site U1356 being likely summer-biased, and deep-water formation likely occurring during wintertime and not exactly in the region of U1356, gives confidence that there is indeed a relation between Southern Ocean SSTs and benthic $\delta^{18}O$ values. Although not yet quantifiable due to the above-mentioned uncertainties, this relation will have implications for $\delta^{18}O$-based ice-volume reconstructions. Therefore, we have conducted a thought experiment by ignoring the uncertainties in the TEX_{86}-based SST record resulting from low sampling resolution and poor age model, and by assuming the reconstructed SST trend has been relayed to the deep ocean. Then, the reconstructed 1°C cooling in the TEX_{86}-based SST between 30.5 and 27 Ma could account for one third of the about 0.75‰ $\delta^{18}O$ long-term decrease between 32 and 27 Ma (1°C = 0.21-0.23‰; Ravelo & Hillaire-Marcel 2007). Similarly, the late Oligocene warming of 1.5°C in our SST record between 27 and 25 Ma would account for much of the coeval 0.50‰ decrease in $\delta^{18}O$. However, the further 0.02‰ decrease of benthic $\delta^{18}O$ between 25 and 24 Ma should then be related to ice volume loss, since our SWTs decrease with 2°C at that time. Recent ice-volume calculations by Liebrand et al. (2017) suggest that the ice-sheet volume around 27 Ma is at least as large as today's East Antarctic ice sheet, assuming deep-sea temperatures cannot drop below current bottom-water temperatures (Fig. 4). However, because their calculations are also based on a constant deep-sea temperature, they are overestimating the long-term growth and decline between 32 and 25 Ma (Liebrand et al., 2017). Hence, if the magnitude of deep-sea temperature long-term change is equal to our long-term reconstructed SST trends, current ice-volume estimates during periods of low benthic $\delta^{18}O$ (see Fig. 4) are underestimating the size of the Antarctic ice sheet. After 24 Ma, and towards Mi-1, the long-term $\delta^{18}O$ trend rises 0.6‰, while the reconstructed SST trends drop about 3°C. Although this cooling could fully account for the long-term $\delta^{18}O$ trend between 24 and 23 Ma, we

Clim. Past Discuss., https://doi.org/10.5194/cp-2017-153
Manuscript under review for journal Clim. Past
Discussion started: 14 December 2017

435 acknowledge the existing physical evidence for a profound glaciation event during Mi-1 (Naish et al., 2001). Similarly, we fully recognize that ice volume variability took place during the Oligocene on the long term (Liebrand et al., 2017; Pekar et al., 2006; Pekar and Christie-Blick, 2008), but we suggest that ice-volume variability before 24 Ma was less than previously assumed, as part of the variation has to be attributed to likely changes in deep-sea temperatures over these timescales.

440 4.3 Sea surface temperature variability at glacial–interglacial time scales

The offset between the glacial and interglacial LOESS curves is constant over time (Fig. 4). Irrespective of the chosen calibration (i.e. TEX_{86} or BAYSPAR), SSTs are on average 1.8-3.2°C higher during interglacial intervals than during adjacent glacial times. This glacial-interglacial SST difference is smaller than the observed amplitude of the variability in our temperature record (2σ = 3.6°C before 27 Ma), because it takes relatively warm glacials and
445 cool interglacial SST values into account. Also considering that part of the 2σ variability is due to the relatively large calibration error of the BAYSPAR calibration (±3.5°C), the difference of 1.8-3.2°C may be a better representation of average glacial-interglacial SST variation than the 2σ. If such glacial-interglacial SST variability is representative for the wider Southern Ocean region and relayed to the deep-sea, it should be considered when interpreting benthic foraminiferal $\delta^{18}O$ records in terms of ice-volume variability. As such, a larger variability of
450 $\delta^{18}O$ than so far assumed (Liebrand et al., 2017; Hauptvogel et al., 2017) should be ascribed to deep-sea temperature rather than ice-volume changes. To be more specific, 40-70% of the 1‰ deep-sea $\delta^{18}O$ variability over Oligocene glacial-interglacial cycles can be related to deep-sea temperature (Fig. 5). However, it is likely that not the entire amplitude of SST variability is relayed to the deep-sea. Indeed, Mg/Ca-based reconstructed bottom-water temperatures from Site 1218 show much less glacial-interglacial variation (1.13°C, Fig. 5) (Lear et al., 2004). This
455 suggests that the amplitude of the glacial-interglacial temperature variation of the surface ocean is strongly reduced at the nearby bottom-water formation sites. Likely, because bottom water has likely formed in the subsurface during winter like today (Baines, 2009; Jacobs, 1991). Still, our record provides additional evidence that polar SST experienced considerable variability, both on the short-term glacial-interglacial cycles as well as on the long-term. Our data furthermore suggest that glacial-interglacial SST variability increased after 27 Ma (Fig. 3B), which
460 suggests a lower contribution of ice volume to the deep-sea $\delta^{18}O$ signal during the late Oligocene. A major influence of deep-sea temperature on benthic $\delta^{18}O$ could explain the level of symmetry in glacial-interglacial cycles in the Oligocene (Liebrand et al., 2017), as the temperature would vary in a sinusoidal fashion, whereas ice sheets would respond non-linearly to climate forcing. Note that this reasoning is still rather speculative as the sedimentary record of Site U1356 lacks the potential to obtain a resolution comparable to that of deep-sea $\delta^{18}O$ records. However, ice-
465 volume reconstructions from $\delta^{18}O$ records on both long-term and short-term time scales should consider that an important component of the signal could potentially be ascribed to temperature variability.

4.4 Implication for the Antarctic Circumpolar Current

Clim. Past Discuss., https://doi.org/10.5194/cp-2017-153
Manuscript under review for journal Clim. Past
Discussion started: 14 December 2017

Today the ACC and the associated Antarctic divergence isolate the continent from lower-latitude influence and are keeping sea-surface temperatures south of the divergence relatively cool (Orsi et al., 1995). The strength and development of the ACC during the Oligocene co-depends on the opening (and depth) of the Tasmanian Gateway and Drake Passage (Hill et al., 2013). If the Tasmanian Gateway and the Drake Passage were open to allow for some deep-water throughflow during the Oligocene, modeling of ocean currents suggests that a strong ACC could only develop once the ocean gateways are in line with the latitudinal position of the westerly winds (Hill et al., 2013). Dinoflagellate cysts (Stickley et al., 2004) and neodymium isotopes from east and west of Tasmania (Scher et al., 2015) indicate that significant eastward throughflow started south of Tasmania around 35-30 Ma. Instead, the TEX_{86}-based SST record and dinoflagellate cyst record (Bijl et al., this issue) of Site U1356 suggest an influence of these warmer northerly waters also at higher latitudes. This suggests that Site U1356 is not fully isolated by a strong flowing ACC and that the eastward flowing current south of Tasmania might have been deflected towards Site U1356. Alternatively, warmer surface water may have reached Site U1356 through eddy-induced heat transport (Dufour et al., 2015; Thompson et al., 2014). It remains a matter of debate when Drake Passage opened sufficiently to allow for a significant ACC throughflow (Lawver & Gahagan 2003; Livermore et al. 2004; Scher & Martin 2006; 2008; Barker et al. 2007; Lagabrielle et al. 2009; Maldonado et al. 2014; Dalziel 2014). Depending on whether Drake Passage was closed or open, modeling suggests that the westward flowing ACCC was stronger or weaker, respectively (Hill et al., 2013). Site U1356 would then be respectively more or less under the influence of the ACCC. If Drake Passage was closed, a stronger ACCC would be able to transport the warm waters recorded at Site U1356 further along the Antarctic coastal margin and thereby explain also the relatively warm temperatures at Site 689.

5 Conclusions

We reconstruct a summer SST of around 17°C on average for the Wilkes Land Margin during the Oligocene, albeit with much variability (up to a 6.8°C double standard deviation during the late Oligocene). The reconstructed temperatures are a few degrees higher than published high-latitude early Oligocene Southern Ocean estimates. Because alternations in the lithology reflect glacial-interglacial cycles, an estimated temperature difference of 2 to 3°C between glacials and interglacials could be determined. The long-term trends of both glacial and interglacial records show a temperature increase towards 30.5 Ma and a decrease after 25 Ma, generally following the long-term trends in the benthic $\delta^{18}O$ record. Our results suggest that considerable SST variability prevailed during the Oligocene, which might have implications for the dynamics of marine-based continental ice sheets, if present, and the extent of the Antarctic ice sheet in general. Assuming that the reconstructed SST trends and glacial-interglacial variability have been relayed to the deep water at nearby bottom-water formation sites, our results imply that the long-term $\delta^{18}O$ trend may for a considerable part be controlled by bottom-water temperature in addition to ice-volume fluctuations. This would mean that the Antarctic ice sheet was less sensitive to polar climate changes than previously assumed.

6 Acknowledgements

JDH, FS and PKB acknowledge NWO Netherlands Polar Program project number 866.10.110. SS was supported by the Netherlands Earth System Science Centre (NESSC), funded by the Dutch Ministry of Education, Culture and Science (OCW). PKB and FP received funding through NWO-ALW VENI grant no 863.13.002 and 863.13.016, respectively. CE and AS thank the Spanish Ministerio de Economía y Competitividad for Grant CTM2014-60451-C2-1-P. We thank Alexander Ebbingh and Anja Bruls for help with the GDGT sample preparation. Henk Brinkhuis is thanked for useful discussions.

7 Author contributions

FS, PKB and SS designed the research. JDH, PKB and AJPH carried out GDGT analyses. CE and AS incorporated the lithological data. PKB, FP and SS assisted in GDGT analytical procedures and interpretation. JDH wrote the paper with input from all authors.

8 References

Austermann, J., Pollard, D., Mitrovica, J.X., Moucha, R., Forte, A.M., DeConto, R.M., Rowley, D.B., Raymo, M.E., 2015. The impact of dynamic topography change on Antarctic ice sheet stability during the mid-Pliocene warm period. Geology 43, 927–930. https://doi.org/10.1130/G36988.1

Baines, P.G., 2009. A model for the structure of the Antarctic Slope Front. Deep. Res. Part II 56, 859–873. https://doi.org/10.1016/j.dsr2.2008.10.030

Barker, P.F., Filippelli, G.M., Florindo, F., Martin, E.E., Scher, H.D., 2007. Onset and role of the Antarctic Circumpolar Current. Deep Sea Res. Part II Top. Stud. Oceanogr. 54, 2388–2398. https://doi.org/10.1016/j.dsr2.2007.07.028

Basse, A., Zhu, C., Versteegh, G.J.M., Fischer, G., Hinrichs, K.-U., 2014. Distribution of intact and core tetraether lipids in water column profiles of suspended particulate matter off Cape Blanc , NW Africa. Org. Geochem. 72, 1–13. https://doi.org/10.1016/j.orggeochem.2014.04.007

Beddow, H.M., Liebrand, D., Sluijs, A., Wade, B.S., Lourens, L.J., 2016. Global change across the Oligocene-Miocene transition: High-resolution stable isotope records from IODP Site U1334 (equatorial Pacific Ocean). Paleoceanography 31, 81–97. https://doi.org/10.1002/2015PA002820.Received

Bijl, P.K., Bendle, J.A.P., Bohaty, S.M., Pross, J., Schouten, S., Tauxe, L., Stickley, C.E., McKay, R.M., Röhl, U., Olney, M., Sluijs, A., Escutia, C., Brinkhuis, H., 2013. Eocene cooling linked to early flow across the Tasmanian Gateway. Proc. Natl. Acad. Sci. U. S. A. 110, 9645–9650. https://doi.org/10.1073/pnas.1220872110

Bijl, P.K., Pross, J., Warnaar, J., Stickley, C.E., Huber, M., Guerstein, R., Houben, A.J.P., Sluijs, A., Visscher, H., Brinkhuis, H., 2011. Environmental forcings of Paleogene Southern Ocean dinoflagellate biogeography. Paleoceanography 26, PA1202. https://doi.org/10.1029/2009PA001905

Bijl, P.K., Houben, A.J.P., Bruls, A., Hartman, J.D., Pross, J., Salabarnada, A., Escutia, C., Sangiorgi, F., submitted

this volume. Oligocene–Miocene paleoceanography off the Wilkes Land Margin (East Antarctica) based on organic-walled dinoflagellate cysts.

Bijl, P.K., Houben, A.J.P., Bruls, A., Pross, J., Sangiorgi, F., accepted manuscript. Stratigraphic calibration of Oligocene-Miocene organic-walled dinoflagellate cysts from offshore Wilkes Land, East Antarctica and a zonation proposal.

Blaga, C.I., Reichart, G.-J., Heiri, O., Sinninghe Damsté, J.S., 2009. Tetraether membrane lipid distributions in water-column particulate matter and sediments: a study of 47 European lakes along a north–south transect. J. Paleolimnol. 41, 523–540. https://doi.org/10.1007/s10933-008-9242-2

Borrelli, C., Katz, M.E., 2015. Dynamic deepwater circulation in the northwestern Pacific during the Eocene: Evidence from ODP Site 884 benthic foraminiferal stable isotopes (δ18O and δ13C). Geosphere, 11, 1204–1225. doi:10.1130/GES01152.1.

Carter, L., Carter, R.M., McCave, I.N., 2004. Evolution of the sedimentary system beneath the deep Pacific inflow off eastern New Zealand. Mar. Geol. 205, 9–27. https://doi.org/10.1016/S0025-3227(04)00016-7

Church, M.J., DeLong, E.F., Ducklow, H.W., Karner, M.B., Preston, C.M., Karl, D.M., 2003. Abundance and distribution of planktonic Archaea and Bacteria in the waters west of the Antarctic Peninsula. Limnol. Oceanogr. 48, 1893–1902. https://doi.org/10.4319/lo.2003.48.5.1893

Church, M.J., Wai, B., Karl, D.M., DeLong, E.F., 2010. Abundances of crenarchaeal amoA genes and transcripts in the Pacific Ocean. Environ. Microbiol. 12, 679–688. https://doi.org/10.1111/j.1462-2920.2009.02108.x

Cleveland, W. S., Grosse, E., Shyu, W. M., 1992. Local regression models. In Chambers, J. M. and Hastie, T. J. (eds.) , Statistical Models in S, chapter 8, 309–376. Chapman & Hall, New York.

Cramer, B.S., Toggweiler, J.R., Wright, J.D., Katz, M.E., Miller, K.G., 2009. Ocean overturning since the late cretaceous: Inferences from a new benthic foraminiferal isotope compilation. Paleoceanography 24, 1–14. https://doi.org/10.1029/2008PA001683

Crampton, J.S., Cody, R.D., Levy, R., Harwood, D., Mckay, R., Naish, T.R., 2016. Southern Ocean phytoplankton turnover in response to stepwise Antarctic cooling over the past 15 million years 113. https://doi.org/10.1073/pnas.1600318113

Dalziel, I.W.D., 2014. Drake Passage and the Scotia arc: A tortuous space-time gateway for the Antarctic Circumpolar Current. Geology 42, 367–368. https://doi.org/10.1130/focus042014.1

Deconto, R.M., Pollard, D., 2016. Contribution of Antarctica to past and future sea-level rise. Nature 531, 591–597. https://doi.org/10.1038/nature17145

DeConto, R.M., Pollard, D., Wilson, P.A., Pälike, H., Lear, C.H., Pagani, M., 2008. Thresholds for Cenozoic bipolar glaciation. Nature 455, 652–656. https://doi.org/10.1038/nature07337

Douglas, P.M.J., Affek, H.P., Ivany, L.C., Houben, A.J.P., Sijp, W.P., Sluijs, A., Schouten, S., Pagani, M., 2014. Pronounced zonal heterogeneity in Eocene southern high-latitude sea surface temperatures. Proc. Natl. Acad. Sci. U. S. A. 111, 1–6. https://doi.org/10.1073/pnas.1321441111

Dufour, C.O., Griffies, S.M., de Souza, G.F., Frenger, I., Morrison, A.K., Palter, J.B., Sarmiento, J.L., Galbraith, E.D., Dunne, J.P., Anderson, W.G., Slater, R.D., 2015. Role of Mesoscale Eddies in Cross-Frontal

Transport of Heat and Biogeochemical Tracers in the Southern Ocean. J. Phys. Oceanogr. 45, 3057–3081. https://doi.org/10.1175/JPO-D-14-0240.1

Elderfield, H., Yu, J., Anand, P., Kiefer, T., Nyland, B., 2006. Calibrations for benthic foraminiferal Mg/Ca paleothermometry and the carbonate ion hypothesis. Earth Planet. Sci. Lett. 250, 633–649. https://doi.org/10.1016/j.epsl.2006.07.041

Escutia, C., Brinkhuis, H., Klaus, A., Scientists, the E. 318, 2011. Expedition 318 summary. Proc. Integr. Ocean Drill. Progr. 318, 1–59. https://doi.org/10.2204/iodp.proc.318.101.2011

Esper, O., Zonneveld, K.A.F., 2007. The potential of organic-walled dinoflagellate cysts for the reconstruction of past sea-surface conditions in the Southern Ocean. Mar. Micropaleontol. 65, 185–212. https://doi.org/10.1016/j.marmicro.2007.07.002

Fogwill, C.J., Turney, C.S.M., Meissner, K.J., Golledge, N.R., Spence, P., Roberts, J.L., England, M.H., Jones, R.T., Carter, L., 2014. Testing the sensitivity of the East Antarctic Ice Sheet to Southern Ocean dynamics: past changes and future implications. J. Quat. Sci. 29, 91–98. https://doi.org/10.1002/jqs.2683

Foster, G.L., Rohling, E.J., 2013. Relationship between sea level and climate forcing by CO2 on geological timescales. Proc. Natl. Acad. Sci. 110, 1209–1214. https://doi.org/10.1073/pnas.1216073110

Fretwell, P., Pritchard, H.D., Vaughan, D.G., Bamber, J.L., Barrand, N.E., Bell, R., Bianchi, C., Bingham, R.G., Blankenship, D.D., Casassa, G., Catania, G., Callens, D., Conway, H., Cook, A.J., Corr, H.F.J., Damaske, D., Damm, V., Ferraccioli, F., Forsberg, R., Fujita, S., Gim, Y., Gogineni, P., Griggs, J.A., Hindmarsh, R.C.A., Holmlund, P., Holt, J.W., Jacobel, R.W., Jenkins, A., Jokat, W., Jordan, T., King, E.C., Kohler, J., Krabill, W., Riger-Kusk, M., Langley, K.A., Leitchenkov, G., Leuschen, C., Luyendyk, B.P., Matsuoka, K., Mouginot, J., Nitsche, F.O., Nogi, Y., Nost, O.A., Popov, S. V., Rignot, E., Rippin, D.M., Rivera, A., Roberts, J., Ross, N., Siegert, M.J., Smith, A.M., Steinhage, D., Studinger, M., Sun, B., Tinto, B.K., Welch, B.C., Wilson, D., Young, D.A., Xiangbin, C., Zirizzotti, A., 2013. Bedmap2: Improved ice bed, surface and thickness datasets for Antarctica. Cryosphere 7, 375–393. https://doi.org/10.5194/tc-7-375-2013

Gasson, E., Deconto, R.M., Pollard, D., Levy, R.H., 2016. Dynamic Antarctic ice sheet during the early to mid-Miocene. https://doi.org/10.1073/pnas.1516130113

Goldner, A., Herold, N., Huber, M., 2014. Antarctic glaciation caused ocean circulation changes at the Eocene–Oligocene transition. Nature 511, 574–577. https://doi.org/10.1038/nature13597

Golledge, N.R., Levy, R.H., Mckay, R.M., Naish, T.R., 2017. East Antarctic ice sheet most vulnerable to Weddell Sea warming. Geophys. Res. Lett. 44, 2343–2351. https://doi.org/10.1002/2016GL072422

Gradstein, F.M., Ogg, J.G., Smith, A.G. (Eds.), 2004. A Geologic Time Scale 2004. Cambridge University Press, Cambridge, p. 589.

Gradstein, F.M., Ogg, J.G., Schmitz, M.D., Ogg, G. (Eds.), 2012. The Geologic Time Scale 2012. Elsevier, Boston, USA, p. 1127, DOI: 10.1016/B978-0-444-59425-9.00004-4.

Greenbaum, J.S., Blankenship, D.D., Young, D. a, Richter, T.G., Roberts, J.L., Aitken, a R. a, Legresy, B., Schroeder, D.M., Warner, R.C., van Ommen, T.D., Siegert, M.J., 2015. Ocean access to a cavity beneath Totten Glacier in East Antarctica. Nat. Geosci. 8, 1–5. https://doi.org/10.1038/NGEO2388

Hauptvogel, D.W., Pekar, S.F., Pincay, V., 2017. Evidence for a heavily glaciated Antarctica during the late Oligocene "warming" (27.8-24.5 Ma): Stable isotope records from ODP Site 690. Paleoceanography 32, 384–396. https://doi.org/10.1002/2016PA002972

Hill, D.J., Haywood, A.M., Valdes, P.J., Francis, J.E., Lunt, D.J., Wade, B.S., Bowman, V.C., 2013. Paleogeographic controls on the onset of the Antarctic circumpolar current. Geophys. Res. Lett. 40, 5199–5204. https://doi.org/10.1002/grl.50941

Hinsbergen, D.J.J. Van, Groot, L.V. De, Schaik, S.J. Van, Spakman, W., Bijl, P.K., Sluijs, A., Langereis, C.G., Brinkhuis, H., 2015. A Paleolatitude Calculator for Paleoclimate Studies. PLoS One 10, 1–21. https://doi.org/10.5281/zenodo.16166.

Ho, S.L., Laepple, T., 2016. Flat meridional temperature gradient in the early Eocene in the subsurface rather than surface ocean. Nat. Geosci. 9, 606–610. https://doi.org/10.1038/ngeo2763

Ho, S.L., Mollenhauer, G., Fietz, S., Martínez-Garcia, A., Lamy, F., Rueda, G., Schipper, K., Méheust, M., Rosell-Melé, A., Stein, R., Tiedemann, R., 2014. Appraisal of TEX86 and TEX86L thermometries in subpolar and polar regions. Geochim. Cosmochim. Acta 131, 213–226. https://doi.org/10.1016/j.gca.2014.01.001

Hopmans, E.C., Schouten, S., Sinninghe Damsté, J.S., 2016. Organic Geochemistry The effect of improved chromatography on GDGT-based palaeoproxies. Org. Geochem. 93, 1–6. https://doi.org/10.1016/j.orggeochem.2015.12.006

Hopmans, E.C., Weijers, J.W.H., Schefuß, E., Herfort, L., Sinninghe Damsté, J.S., Schouten, S., 2004. A novel proxy for terrestrial organic matter in sediments based on branched and isoprenoid tetraether lipids. Earth Planet. Sci. Lett. 224, 107–116. https://doi.org/10.1016/j.epsl.2004.05.012

Houben, A.J.P., Bijl, P.K., Guerstein, G.R., Sluijs, A.,Brinkhuis, H., 2011. Malvinia escutiana, a new biostratigraphically important Oligocene dinoflagellate cyst from the Southern Ocean. Rev. Palaeobot. Palynol. 165, 175-182. http://dx.doi.org/10.1016/j.revpalbo.2011.03.002

Houben, A.J.P., Bijl, P.K., Pross, J., Bohaty, S.M., Passchier, S., Stickley, C.E., Röhl, U., Sugisaki, S., Tauxe, L., van de Flierdt, T., Olney, M., Sangiorgi, F., Sluijs, A., Escutia, C., Brinkhuis, H., Dotti, C.E., Klaus, A., Fehr, A., Williams, T., Bendle, J. a P., Carr, S. a, Dunbar, R.B., Flores, J.-A., Gonzàlez, J.J., Hayden, T.G., Iwai, M., Jimenez-Espejo, F.J., Katsuki, K., Kong, G.S., McKay, R.M., Nakai, M., Pekar, S.F., Riesselman, C., Sakai, T., Salzmann, U., Shrivastava, P.K., Tuo, S., Welsh, K., Yamane, M., 2013. Reorganization of Southern Ocean plankton ecosystem at the onset of Antarctic glaciation. Science 340, 341–344. https://doi.org/10.1126/science.1223646

Huguet, C., Hopmans, E.C., Febo-Ayala, W., Thompson, D.H., Sinninghe Damsté, J.S., Schouten, S., 2006. An improved method to determine the absolute abundance of glycerol dibiphytanyl glycerol tetraether lipids. Org. Geochem. 37, 1036–1041. https://doi.org/10.1016/j.orggeochem.2006.05.008

IPCC, 2014. Climate Change 2014: Synthesis Report. Contribution of Working Groups I, II and III to the Fifth Assessment Report of the Intergovernmental Panel on Climate Change. IPCC, Geneva, Switzerland.

Jacobs, S.S., 1991. On the nature and significance of the Antarctic Slope Front. Mar. Chem. 35, 9–24. https://doi.org/10.1016/S0304-4203(09)90005-6

Joughin, I., Smith, B.E., Medley, B., 2014. Marine Ice Sheet Collapse Potentially Under Way for the Thwaites Glacier Basin, West Antarctica. Science (80-.). 344, 735–738. https://doi.org/10.1126/science.1249055

Kalanetra, K.M., Bano, N., Hollibaugh, J.T., 2009. Ammonia-oxidizing Archaea in the Arctic Ocean and Antarctic coastal waters. Environ. Microbiol. 11, 2434–2445. https://doi.org/10.1111/j.1462-2920.2009.01974.x

Karner, M.B., DeLong, E.F., Karl, D.M., 2001. Archaeal dominance in the mesopelagic zone of the Pacific Ocean. Nature 409, 507–510. https://doi.org/10.1038/35054051

Katz, M.E., Cramer, B.S., Toggweiler, J.R., Esmay, G., Liu, C., Miller, K.G., Rosenthal, Y., Wade, B.S., Wright, J.D., 2011. Impact of Antarctic Circumpolar Current development on late Paleogene ocean structure. Science (80-.). 332, 1076–1079. https://doi.org/10.1126/science.1202122

Kelson, J.R., Huntington, K.W., Schauer, A.J., Saenger, C., Lechler, A.R., 2017. Toward a universal carbonate clumped isotope calibration : Diverse synthesis and preparatory methods suggest a single temperature relationship. Geochim. Cosmochim. Acta 197, 104–131. https://doi.org/10.1016/j.gca.2016.10.010

Kim, J.-H., Crosta, X., Willmott, V., Renssen, H., Bonnin, J., Helmke, P., Schouten, S., Sinninghe Damsté, J.S., 2012a. Holocene subsurface temperature variability in the eastern Antarctic continental margin. Geophys. Res. Lett. 39. https://doi.org/10.1029/2012GL051157

Kim, J.-H., Romero, O.E., Lohmann, G., Donner, B., Laepple, T., Haam, E., Damsté, J.S.S., 2012b. Pronounced subsurface cooling of North Atlantic waters off Northwest Africa during Dansgaard – Oeschger interstadials. Earth Planet. Sci. Lett. 339–340, 95–102. https://doi.org/10.1016/j.epsl.2012.05.018

Kim, J.-H., Schouten, S., Hopmans, E.C., Donner, B., Sinninghe Damsté, J.S., 2008. Global sediment core-top calibration of the TEX86 paleothermometer in the ocean. Geochim. Cosmochim. Acta 72, 1154–1173. https://doi.org/10.1016/j.gca.2007.12.010

Kim, J.-H., van der Meer, J., Schouten, S., Helmke, P., Willmott, V., Sangiorgi, F., Koç, N., Hopmans, E.C., Damsté, J.S.S., 2010. New indices and calibrations derived from the distribution of crenarchaeal isoprenoid tetraether lipids: Implications for past sea surface temperature reconstructions. Geochim. Cosmochim. Acta 74, 4639–4654. https://doi.org/10.1016/j.gca.2010.05.027

Kim, J., Villanueva, L., Zell, C., Sinninghe Damsté, J.S., 2016. Biological source and provenance of deep-water derived isoprenoid tetraether lipids along the Portuguese continental margin. Geochim. Cosmochim. Acta 172, 177–204. https://doi.org/10.1016/j.gca.2015.09.010

Koga, Y., Morii, H., Akagawa-Matsushita, M., Ohga, M., 1998. Correlation of Polar Lipid Composition with 16S rRNA Phylogeny in Methanogens. Further Analysis of Lipid Component Parts. Bioscience, Biotechnology and Biochemistry 62(2), 230-236.

Lagabrielle, Y., Malavieille, J., Suárez, M., 2009. The tectonic history of Drake Passage and its possible impacts on global climate. Earth Planet. Sci. Lett. 279, 197–211. https://doi.org/10.1016/j.epsl.2008.12.037

Lawver, L.A., Gahagan, L.M., 2003. Evolution of cenozoic seaways in the circum-antarctic region. Palaeogeogr. Palaeoclimatol. Palaeoecol. 198, 11–37. https://doi.org/10.1016/S0031-0182(03)00392-4

Lear, C.H., Mawbey, E.M., Rosenthal, Y., 2010. Cenozoic benthic foraminiferal Mg/Ca and Li/Ca records: Toward unlocking temperatures and saturation states. Paleoceanography 25, 1–11.

https://doi.org/10.1029/2009PA001880

Lear, C.H., Rosenthal, Y., Coxall, H.K., Wilson, P.A., 2004. Late Eocene to early Miocene ice sheet dynamics and the global carbon cycle. Paleoceanography 19, PA4015. https://doi.org/10.1029/2004PA001039

Liebrand, D., Bakker, A.T.M. De, Beddow, H.M., Wilson, P.A., Bohaty, S.M., 2017. Evolution of the early Antarctic ice ages. PNAS 114, 3867–3872. https://doi.org/10.1073/pnas.1615440114

Liebrand, D., Beddow, H.M., Lourens, L.J., Pälike, H., Raffi, I., Bohaty, S.M., Hilgen, F.J., Saes, M.J.M., Wilson, P.A., Dijk, A.E. Van, Hodell, D.A., Kroon, D., Huck, C.E., Batenburg, S.J., 2016. Cyclostratigraphy and eccentricity tuning of the early Oligocene oxygen and carbon isotope records from Walvis Ridge Site 1264. Earth Planet. Sci. Lett. 1, 1–14. https://doi.org/10.1016/j.epsl.2016.06.007

Liebrand, D., Lourens, L.J., Hodell, D.A., De Boer, B., Van De Wal, R.S.W., Pälike, H., 2011. Antarctic ice sheet and oceanographic response to eccentricity forcing during the early Miocene. Clim. Past 7, 869–880. https://doi.org/10.5194/cp-7-869-2011

Liu, Z., Pagani, M., Zinniker, D., DeConto, R., Huber, M., Brinkhuis, H., Shah, S.R., Leckie, R.M., Pearson, A., 2009. Global Cooling During the Eocene-Oligocene Climate Transition. Science (80-.). 323, 1187–1190. https://doi.org/10.1126/science.1166368

Livermore, R., Eagles, G., Morris, P., Maldonado, A., 2004. Shackleton Fracture Zone: No barrier to early circumpolar ocean circulation. Geology 32, 797–800. https://doi.org/10.1130/G20537.1

Locarnini, R.A., Mishonov, A.V., Antonov, J.I., Boyer, T.P., Garcia, H.E., Baranova, O.K., Zweng, M.M., Johnson, D.R., 2010. World Ocean Atlas 2009, Volume 1 : Temperature, NOAA Atlas NESDIS 68. U.S. Government Printing Office, Washington, D.C.

Lopes dos Santos, R.A., Prange, M., Castañeda, I.S., Schefuß, E., Mulitza, S., Schulz, M., Niedermeyer, E.M., Sinninghe, J.S., Schouten, S., 2010. Glacial – interglacial variability in Atlantic meridional overturning circulation and thermocline adjustments in the tropical North Atlantic. Earth Planet. Sci. Lett. 300, 407–414. https://doi.org/10.1016/j.epsl.2010.10.030

Maldonado, A., Bohoyo, F., Galindo-Zaldívar, J., Hernández-Molina, F.J., Lobo, F.J., Lodolo, E., Martos, Y.M., Pérez, L.F., Schreider, A. a., Somoza, L., 2014. A model of oceanic development by ridge jumping: Opening of the Scotia Sea. Glob. Planet. Change 123, 152–173. https://doi.org/10.1016/j.gloplacha.2014.06.010

Maldonado, A., Barnolas, A., Bohoyo, F., Galindo-Zaldívar, J., Hernández-Molina, J., Lobo, F., Rodríguez-Fernández, J., Somoza, L., Vázquez, J.T., 2003. Contourite deposits in the central Scotia Sea: the importance of the Antarctic Circumpolar Current and the Weddell Gyre flows. Palaeogeography, Palaeoclimatology, Palaeoecology 198, 187-221.

Marret, F., De Vernal, A., 1997. Dinoflagellate cyst distribution in surface sediments of the southern Indian Ocean. Mar. Micropaleontol. 29, 367–392. https://doi.org/10.1016/S0377-8398(96)00049-7

Mcmillan, M., Shepherd, A., Sundal, A., Briggs, K., Muir, A., Ridout, A., Hogg, A., Wingham, D., 2014. Increased ice losses from Antarctica detected by CryoSat-2. Geophys. Res. Lett. 41, 3899–3906. https://doi.org/10.1002/2014GL060111.Received

Miles, B.W.J., Stokes, C.R., Jamieson, S.S.R., 2016. Pan – ice-sheet glacier terminus change in East Antarctica reveals sensitivity of Wilkes Land to sea-ice changes. Sci. Adv. 2, e1501350.

Mollenhauer, G., Basse, A., Kim, J.H., Sinninghe Damsté, J.S., Fischer, G., 2015. A four-year record of UK'37- and TEX86-derived sea surface temperature estimates from sinking particles in the filamentous upwelling region off Cape Blanc, Mauritania. Deep. Res. Part I Oceanogr. Res. Pap. 97, 67–79. https://doi.org/10.1016/j.dsr.2014.11.015

Murray, A.E., Preston, C.M., Massana, R., Taylor, T.L., Blakis, A., Wu, K., Delong, E.F., 1998. Seasonal and spatial variability of bacterial and archaeal assemblages in the coastal waters near Anvers Island, Antarctica. Appl. Environ. Microbiol. 64, 2585–2595.

Naish, T.R., Woolfe, K.J., Barrett, P.J., Wilson, G.S., Atkins, C., Bohaty, S.M., Bücker, C.J., Claps, M., Davey, F.J., Dunbar, G.B., Dunn, A.G., Fielding, C.R., Florindo, F., Hannah, M.J., Harwood, D.M., Henrys, S.A., Krissek, L.A., Lavelle, M., van Der Meer, J., McIntosh, W.C., Niessen, F., Passchier, S., Powell, R.D., Roberts, A.P., Sagnotti, L., Scherer, R.P., Strong, C.P., Talarico, F., Verosub, K.L., Villa, G., Watkins, D.K., Webb, P.N., Wonik, T., 2001. Orbitally induced oscillations in the East Antarctic ice sheet at the Oligocene/Miocene boundary. Nature 413, 719–23. https://doi.org/10.1038/35099534

Orsi, A.H., Whitworth, T., Nowlin, W.D., 1995. On the meridional extent and fronts of the Antarctic Circumpolar Current. Deep Sea Res. Part I Oceanogr. Res. Pap. 42, 641–673. https://doi.org/10.1016/0967-0637(95)00021-W

Pagani, M., Huber, M., Liu, Z., Bohaty, S.M., Henderiks, J., Sijp, W., Krishnan, S., DeConto, R.M., 2011. The Role of Carbon Dioxide During the Onset of Antarctic Glaciation. Science (80-.). 334, 1261–1265. https://doi.org/10.1126/science.1203909

Pälike, H., Norris, R.D., Herrle, J.O., Wilson, P.A., Coxall, H.K., Lear, C.H., Shackleton, N.J., Tripati, A.K., Wade, B.S., 2006. The Heartbeat of the Oligocene Climate System. Science (80-.). 314, 1894–1898. https://doi.org/10.1126/science.1133822

Parrenin, F., Masson-Delmotte, V., Köhler, P., Raynaud, D., Paillard, D., Schwander, J., Barbante, C., Landais, A., Wegner, A., Jouzel, J., 2013. Synchronous Change of Atmospheric CO2 and Antarctic Temperature During the Last Deglacial Warming. Science (80-.). 339, 1060–1063.

Passchier, S., Krissek, L.A., 2008. Oligocene-Miocene Antarctic continental weathering record and paleoclimatic implications, Cape Roberts drilling Project, Ross Sea, Antarctica. Palaeogeography, Palaeoclimatology, Palaeoecology 260, 30-40.

Pekar, S.F., Christie-Blick, N., 2008. Resolving apparent conflicts between oceanographic and Antarctic climate records and evidence for a decrease in pCO2 during the Oligocene through early Miocene (34–16 Ma). Palaeogeogr. Palaeoclimatol. Palaeoecol. 260, 41–49. https://doi.org/10.1016/j.palaeo.2007.08.019

Pekar, S.F., DeConto, R.M., Harwood, D.M., 2006. Resolving a late Oligocene conundrum: Deep-sea warming and Antarctic glaciation. Palaeogeogr. Palaeoclimatol. Palaeoecol. 231, 29–40. https://doi.org/10.1016/j.palaeo.2005.07.024

Peterse, F., Kim, J., Schouten, S., Klitgaard, D., Koç, N., Sinninghe, J.S., 2009. Constraints on the application of the

MBT / CBT palaeothermometer at high latitude environments (Svalbard , Norway). Org. Geochem. 40, 692–699. https://doi.org/10.1016/j.orggeochem.2009.03.004

Petersen, S. V., Schrag, D.P., 2015. Antarctic ice growth before and after the Eocene-Oligocene Transition: New estimates from clumped isotope paleothermometry. Paleoceanography n/a-n/a. https://doi.org/10.1002/2014PA002769

Plancq, J., Mattioli, E., Pittet, B., Simon, L., Grossi, V., 2014. Productivity and sea-surface temperature changes recorded during the late Eocene-early Oligocene at DSDP Site 511 (South Atlantic). Palaeogeogr. Palaeoclimatol. Palaeoecol. 407, 34–44. https://doi.org/10.1016/j.palaeo.2014.04.016

Pollard, D., Deconto, R.M., Alley, R.B., 2015. Potential Antarctic Ice Sheet retreat driven by hydrofracturing and ice cliff failure. Earth Planet. Sci. Lett. 412, 112–121. https://doi.org/10.1016/j.epsl.2014.12.035

Prebble, J.G., Crouch, E.M., Carter, L., Cortese, G., Bostock, H., Neil, H., 2013. An expanded modern dinoflagellate cyst dataset for the Southwest Pacific and Southern Hemisphere with environmental associations. Mar. Micropaleontol. 101, 33–48. https://doi.org/10.1016/j.marmicro.2013.04.004

Pritchard, H.D., Ligtenberg, S.R.M., Fricker, H.A., Vaughan, D.G., van den Broeke, M.R., Padman, L., 2012. Antarctic ice-sheet loss driven by basal melting of ice shelves. Nature 484, 502–505. https://doi.org/10.1038/nature10968

Pross, J., Contreras, L., Bijl, P.K., Greenwood, D.R., Bohaty, S.M., Schouten, S., Bendle, J. a, Röhl, U., Tauxe, L., Raine, J.I., Huck, C.E., van de Flierdt, T., Jamieson, S.S.R., Stickley, C.E., van de Schootbrugge, B., Escutia, C., Brinkhuis, H., 2012. Persistent near-tropical warmth on the Antarctic continent during the early Eocene epoch. Nature 488, 73–7. https://doi.org/10.1038/nature11300

Ravelo, A.C., Hillaire-Marcel, C., 2007. The Use of Oxygen and Carbon Isotopes of Foraminifera in Paleoceanography, in: Developments in Marine Geology. Elsevier B.V., pp. 735–764. https://doi.org/10.1016/S1572-5480(07)01023-8

Richey, J.N., Tierney, J.E., 2016. GDGT and alkenone flux in the northern Gulf of Mexico: Implications for the TEX86 and Uk'37 paleothermometers. Paleoceanography 31, 1547–1561. https://doi.org/10.1002/2016PA003032

Rodrigo-Gámiz, M., Rampen, S.W., de Haas, H., Baas, M., Schouten, S., Sinninghe Damsté, J.S., 2015. Constraints on the applicability of the organic temperature proxies UK'37, TEX86 and LDI in the subpolar region around Iceland. Biogeosciences Discuss. 12, 1113–1153. https://doi.org/10.5194/bgd-12-1113-2015

Salabarnada, A., Escutia, C., Röhl, U., Nelson, C.H., McKay, R., Jiménez-Espejo, F.F., Bijl, P.K., Hartman, J.D., Ikehara, M., Strother, S.L., Salzmann, U., Evangelinos, D., López-Quirós, A., Sangiorgi, F., Brinkhuis, H., submitted this volume. Late Oligocene obliquity-paced contourite sedimentation in the Wilkes Land margin of East Antarctica: implications for paleoceanographic and ice sheet configurations.

Scher, H.D., Martin, E.E., 2008. Oligocene deep water export from the North Atlantic and the development of the Antarctic Circumpolar Current examined with neodymium isotopes. Paleoceanography 23, 1–12. https://doi.org/10.1029/2006PA001400

Scher, H.D., Martin, E.E., 2006. Timing and climatic consequences of the opening of Drake Passage. Science (80-.

795). 312, 428–430. https://doi.org/10.1126/science.1120044

Scher, H.D., Whittaker, J.M., Williams, S.E., Latimer, J.C., Kordesch, W.E.C., Delaney, M.L., 2015. Onset of Antarctic Circumpolar Current 30 million years ago as Tasmanian Gateway aligned with westerlies. Nature 523, 580–583. https://doi.org/10.1038/nature14598

Schnack-Schiel, S.B., 2001. Aspects of the study of the life cycles of Antarctic copepods. Hydrobiologia 453–454,
800 9–24. https://doi.org/10.1023/A:1013195329066

Schouten, S., Hopmans, E.C., M, E.S., 2002. Distributional variations in marine crenarchaeotal membrane lipids : a new tool for reconstructing ancient sea water temperatures ? Earth Planet. Sci. Lett. 204, 265–274. https://doi.org/10.1016/S0012-821X(02)00979-2

Schouten, S., Hopmans, E.C., Sinninghe Damsté, J.S., 2013. The organic geochemistry of glycerol dialkyl glycerol
805 tetraether lipids: A review. Org. Geochem. 54, 19–61. https://doi.org/10.1016/j.orggeochem.2012.09.006

Sinninghe Damsté, J.S., 2016. Spatial heterogeneity of sources of branched tetraethers in shelf systems : The geochemistry of tetraethers in the Berau River delta (Kalimantan , Indonesia). Geochim. Cosmochim. Acta 186, 13–31. https://doi.org/10.1016/j.gca.2016.04.033

Sinninghe Damste, J.S., Ossebaar, J., Abbas, B., Schouten, S., Verschuren, D., 2009. Fluxes and distribution of
810 tetraether lipids in an equatorial African lake : Constraints on the application of the TEX 86 palaeothermometer and BIT index in lacustrine settings. Geochim. Cosmochim. Acta 73, 4232–4249. https://doi.org/10.1016/j.gca.2009.04.022

Sluijs, A., Bijl, P.K., Schouten, S., Röhl, U., Reichart, G.-J., Brinkhuis, H., 2011. Southern ocean warming, sea level and hydrological change during the Paleocene-Eocene thermal maximum. Clim. Past 7, 47–61.
815 https://doi.org/10.5194/cp-7-47-2011

Sorlien, C.C., Luyendyk, B.P., Wilson, D.S., Decesari, R.C., Bartek, L.R., Diebold, J.B., 2007. Oligocene development of the West Antarctic Ice Sheet recorded in eastern Ross Sea strata. Geology 35, 467–470. https://doi.org/10.1130/G23387A.1

Spilling, K., Ylöstalo, P., Simis, S., Seppälä, J., 2015. Interaction Effects of Light , Temperature and Nutrient
820 Limitations (N , P and Si) on Growth , Stoichiometry and Photosynthetic Parameters of the Cold-Water Diatom Chaetoceros wighamii. PLoS One 10, e0126308. https://doi.org/10.1371/journal.pone.0126308

Stickley, C.E., Brinkhuis, H., Schellenberg, S.A., Sluijs, A., Röhl, U., Fuller, M., Grauert, M., Huber, M., Warnaar, J., Williams, G.L., 2004. Timing and nature of the deepening of the Tasmanian Gateway. Paleoceanography 19, 1–18. https://doi.org/10.1029/2004PA001022

825 Strother, S.L., Salzmann, U., Sangiorgi, F., Bijl, P.K., Pross, J., Escutia, C., 2017. A new quantitative approach to identify reworking in Eocene to Miocene pollen records from offshore Antarctica using red fluorescence and digital imaging. Biogeosciences 14, 2089–2100. https://doi.org/10.5194/bg-14-2089-2017

Tauxe, L., Stickley, C.E., Sugisaki, S., Bijl, P.K., Bohaty, S.M., Brinkhuis, H., Escutia, C., Flores, J.A., Houben, A.J.P., Iwai, M., Jiménez-Espejo, F., McKay, R., Passchier, S., Pross, J., Riesselman, C.R., Röhl, U.,
830 Sangiorgi, F., Welsh, K., Klaus, A., Fehr, A., Bendle, J.A.P., Dunbar, R., Gonzàlez, J., Hayden, T., Katsuki, K., Olney, M.P., Pekar, S.F., Shrivastava, P.K., van de Flierdt, T., Williams, T., Yamane, M.,

2012. Chronostratigraphic framework for the IODP Expedition 318 cores from the Wilkes Land Margin: Constraints for paleoceanographic reconstruction. Paleoceanography 27, PA2214. https://doi.org/10.1029/2012PA002308

Taylor, K.W.R., Huber, M., Hollis, C.J., Hernandez-Sanchez, M.T., Pancost, R.D., 2013. Re-evaluating modern and Palaeogene GDGT distributions: Implications for SST reconstructions. Glob. Planet. Change 108, 158–174. https://doi.org/10.1016/j.gloplacha.2013.06.011

Thompson, A.F., Heywood, K.J., Schmidtko, S., Stewart, A.L., 2014. Eddy transport as a key component of the Antarctic overturning circulation. Nat. Geosci. 7, 879–884. https://doi.org/10.1038/NGEO2289

Tierney, J.E., Tingley, M.P., 2015. A TEX 86 surface sediment database and extended Bayesian calibration 1–10. https://doi.org/10.1038/sdata.2015.29

Tierney, J.E., Tingley, M.P., 2014. A Bayesian, spatially-varying calibration model for the TEX86 proxy. Geochim. Cosmochim. Acta 127, 83–106. https://doi.org/10.1016/j.gca.2013.11.026

Trommer, G., Siccha, M., van der Meer, M.T.J., Schouten, S., Sinninghe Damsté, J.S., Schulz, H., Hemleben, C., Kucera, M., 2009. Organic Geochemistry Distribution of Crenarchaeota tetraether membrane lipids in surface sediments from the Red Sea. Org. Geochem. 40, 724–731. https://doi.org/10.1016/j.orggeochem.2009.03.001

Villanueva, L., Schouten, S., Damsté, J.S.S., Box, P.O., 2015. Depth-related distribution of a key gene of the tetraether lipid biosynthetic pathway in marine Thaumarchaeota 17, 3527–3539. https://doi.org/10.1111/1462-2920.12508

Wang, Xiao-Feng, 2010. fANCOVA: Non-parametric analysis of covariance. https://CRAN.R-project.org/package=fANCOVA

Weijers, J.W.H., Lim, K.L.H., Aquilina, A., Sinninghe Damsté, J.S., Pancost, R.D., 2011. Biogeochemical controls on glycerol dialkyl glycerol tetraether lipid distributions in sediments characterized by diffusive methane flux. Geochemistry, Geophys. Geosystems 12, Q10010. https://doi.org/10.1029/2011GC003724

Weijers, J.W.H., Schouten, S., Hopmans, E.C., Geenevasen, J.A.J., David, O.R.P., Coleman, J.M., Pancost, R.D., Sinninghe Damsté, J.S., 2006. Membrane lipids of mesophilic anaerobic bacteria thriving in peats have typical archaeal traits. Environ. Microbiol. 8, 648–657. https://doi.org/10.1111/j.1462-2920.2005.00941.x

Wilson, D.S., Jamieson, S.S.R., Barrett, P.J., Leitchenkov, G., Gohl, K., Larter, R.D., 2012. Antarctic topography at the Eocene–Oligocene boundary. Palaeogeogr. Palaeoclimatol. Palaeoecol. 335–336, 24–34. https://doi.org/10.1016/j.palaeo.2011.05.028

Yamamoto, M., Shimamoto, A., Fukuhara, T., Tanaka, Y., Ishizaka, J., 2012. Glycerol dialkyl glycerol tetraethers and TEX86 index in sinking particles in the western North Pacific. Org. Geochem. 53, 52–62. https://doi.org/10.1016/j.orggeochem.2012.04.010

Zachos, J., 2001. Trends, Rhythms, and Aberrations in Global Climate 65 Ma to Present. Science (80-.). 292, 686–693. https://doi.org/10.1126/science.1059412

Zachos, J.C., Dickens, G.R., Zeebe, R.E., 2008. An early Cenozoic perspective on greenhouse warming and carbon-cycle dynamics. Nature 451, 279–283. https://doi.org/10.1038/nature06588

Zhang, Y.G., Pagani, M., Liu, Z., Bohaty, S.M., DeConto, R., 2013. A 40-million-year history of atmospheric CO2. Phil. Trans. R. Soc. A 371, 20130096. https://doi.org/10.1098/rsta.2013.0096

Zhang, Y.G., Pagani, M., Wang, Z., 2016. Ring Index: A new strategy to evaluate the integrity of TEX86 paleothermometry. Paleoceanography 31, 220–232. https://doi.org/10.1002/2015PA002848.Received

Zhang, Y.G., Zhang, C.L., Liu, X., Li, L., Hinrichs, K., Noakes, J.E., 2011. Methane Index : A tetraether archaeal lipid biomarker indicator for detecting the instability of marine gas hydrates 307, 525–534. https://doi.org/10.1016/j.epsl.2011.05.031

Clim. Past Discuss., https://doi.org/10.5194/cp-2017-153
Manuscript under review for journal Clim. Past
Discussion started: 14 December 2017

Climate of the Past
Discussions
Open Access
EGU

Figures 1-5

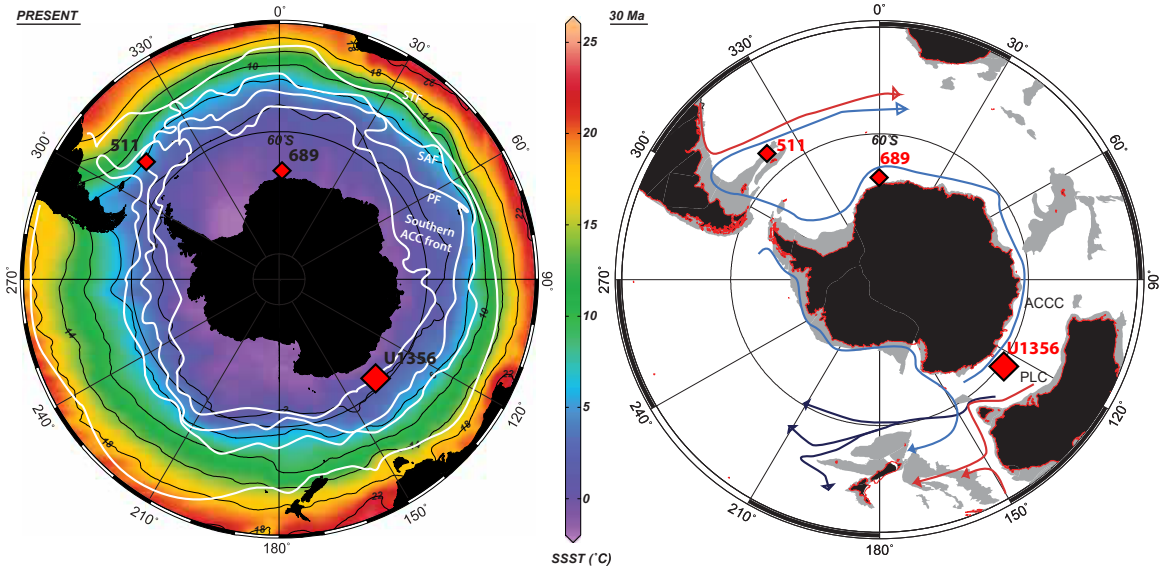

Figure 1: left: Present-day Southern Ocean summer temperatures and geography obtained from the World Ocean Atlas (Locarnini et al., 2010) using Ocean Data View, and Southern Ocean Fronts obtained from Orsi et al. (1995). Right: modified ODSN-generated map of Antarctica around 30 Ma (continents in black, shelf areas in grey). Red diamonds indicate DSDP/ODP/IODP Site locations. Paleolatitudes calculated with paleolatitude.org (Hinsbergen et al. 2015). Reconstructed cold (light blue) and warm (red) surface currents are based on publications by Stickley et al. (2004), Bijl et al. (2011), Bijl et al. (2013), and Douglas et al. (2014). Reconstructed bottom-water currents (dark blue) are based on publications by Carter et al. (2004) and Scher et al. (2015). ACCC = Antarctic Circumpolar Counter Current, PLC = Proto-Leeuwin Current.

Clim. Past Discuss., https://doi.org/10.5194/cp-2017-153
Manuscript under review for journal Clim. Past
Discussion started: 14 December 2017

Climate of the Past Discussions
Open Access
EGU

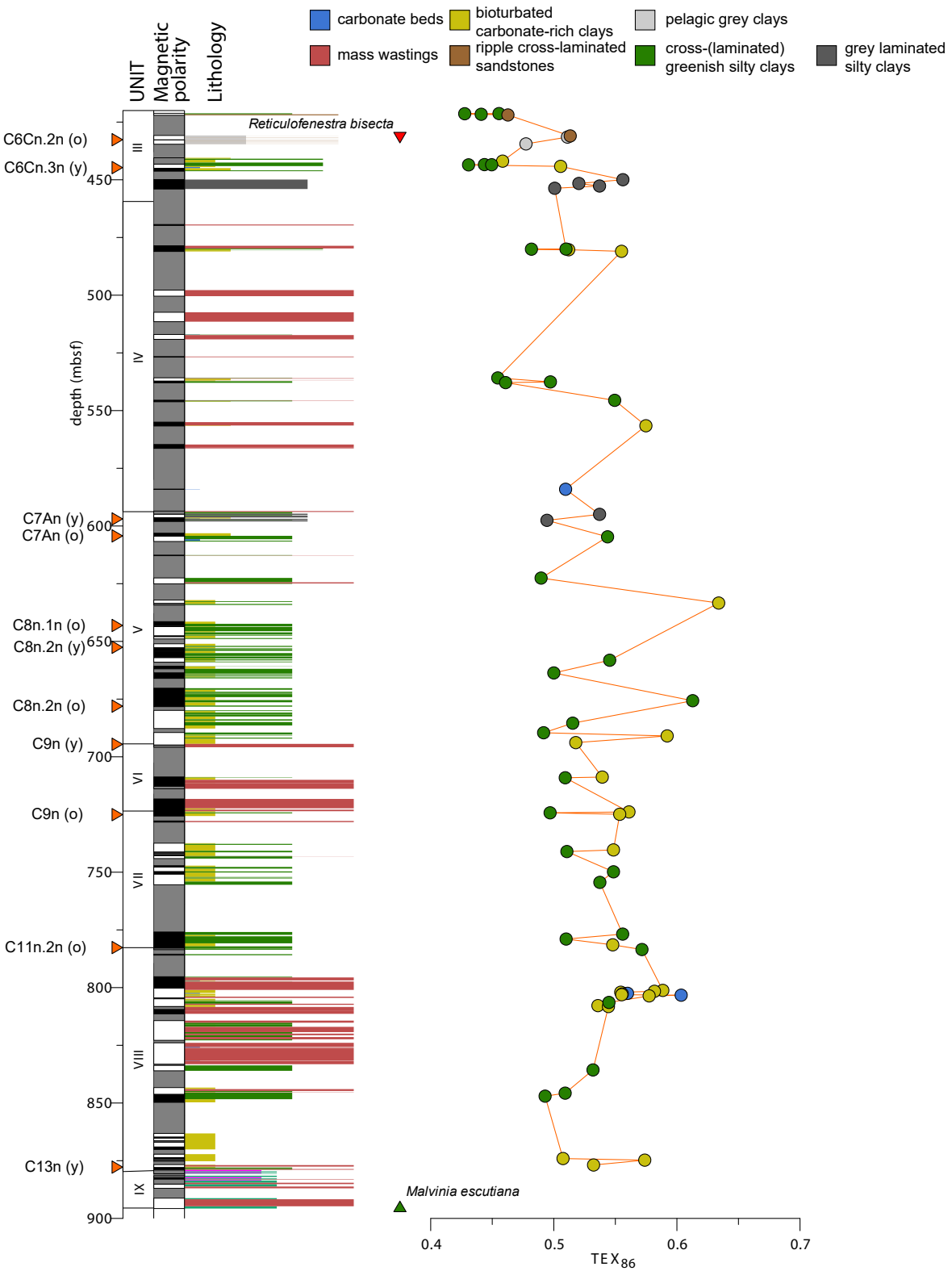

Figure 2: Lithology of Hole U1356A plotted against depth (mbsf) with units according to (Escutia et al., 2011) and chronostratigraphic tie points and paleomagnetic polarities obtained from Tauxe et al. (2012). Depositional facies are indicated with colors in the lithological column (see legend above). Colors of the TEX_{86} index values reflect the lithology they have been sampled from.

Clim. Past Discuss., https://doi.org/10.5194/cp-2017-153
Manuscript under review for journal Clim. Past
Discussion started: 14 December 2017

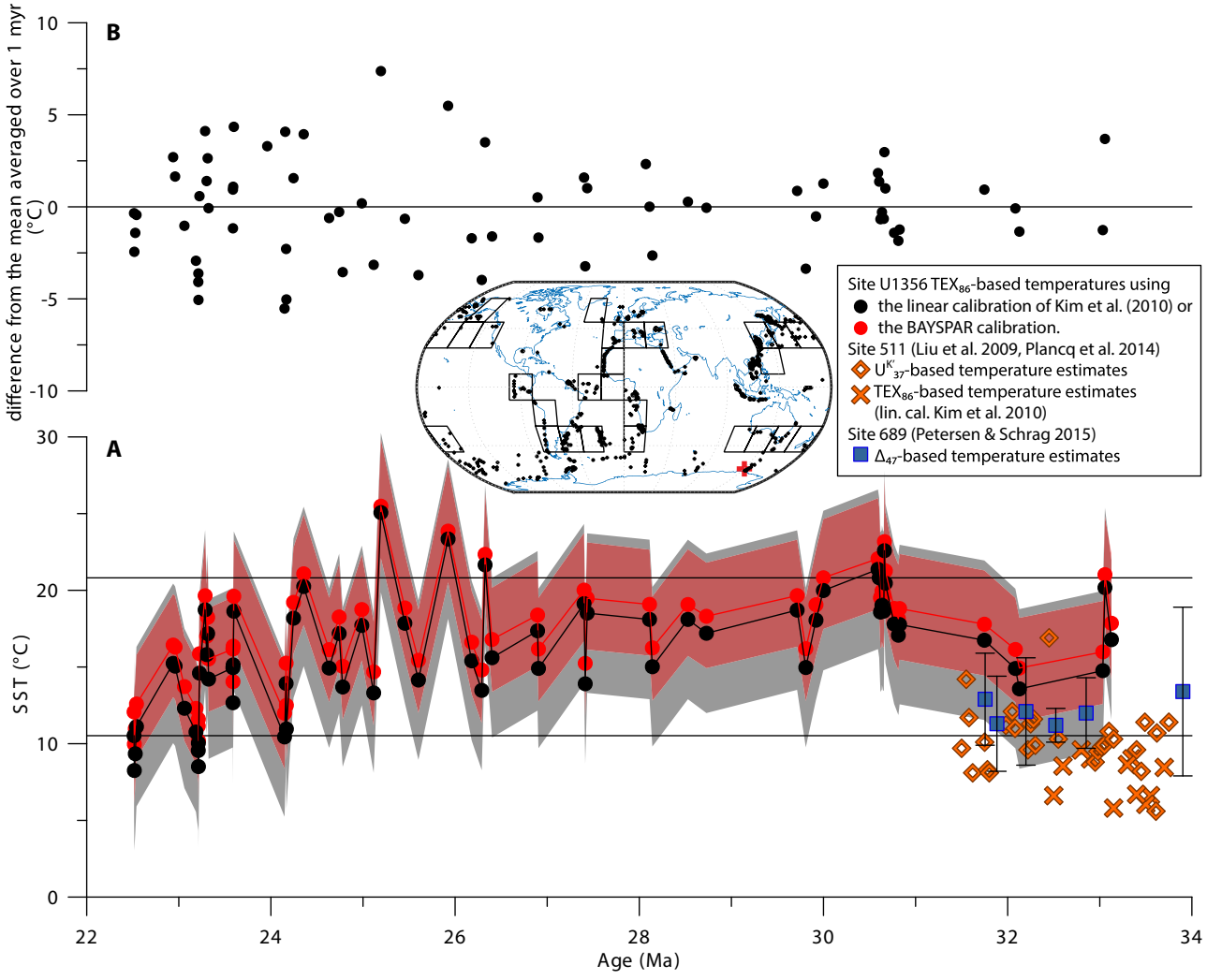

Figure 3: The calibrations to TEX_{86} with corresponding standard errors (as shaded envelopes) (A) using the linear calibration of Kim et al. (2010) (in black) and the Bayesian spatially-varying regression model of Tierney and Tingley (2015) (in red). For the Bayesian calibration the used 20x20° grid cells are indicated in the map (black dots represent surface sediment samples used for the calibration and the red cross is the location of Site U1356), the prior mean is derived from Petersen and Schrag (2015). Also plotted are temperature estimates from Site 511 and Site 689 (A). Differences from the LOESS mean of the SST reconstruction based on the calibration of Kim et al. (2010) are plotted above (B).

Clim. Past Discuss., https://doi.org/10.5194/cp-2017-153
Manuscript under review for journal Clim. Past
Discussion started: 14 December 2017

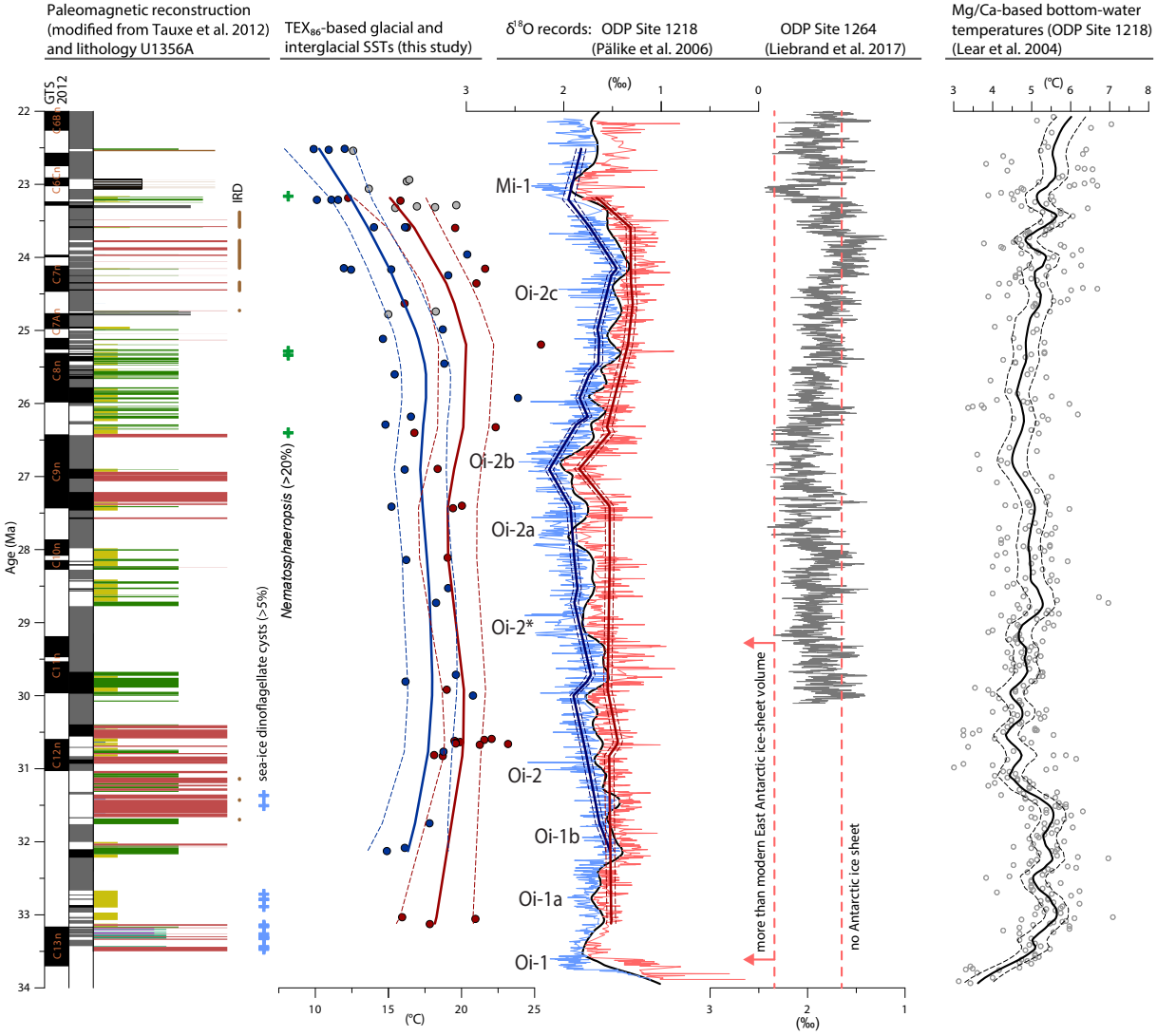

Figure 4: Lithology and paleomagnetic polarities as in Fig. 2, but plotted against age (Ma) updated to the GTS2012 timescale (Gradstein et al. 2012). Sections with IRD, and samples with sea-ice dinoflagellate cysts and *Nematosphaeropsis* dinocysts are indicated. Blue and red dots represent glacial and interglacial TEX_{86}-based SST estimates, respectively, based on the BAYSPAR calibration of Tierney and Tingley (2015). Thick red and blue lines are the LOESS curve averages of these interglacial and glacial SST curves with corresponding 95%-confidence interval (dotted lines). Benthic $\delta^{18}O$ record of Site 1218 according to Pälike et al. (2006). Black LOESS curve average separates glacial (blue) and interglacial (red) $\delta^{18}O$ values. Thick red and blue curves represent the long-term interglacial and glacial trends and 95% confidence intervals (dotted lines), respectively, based on resampling of the $\delta^{18}O$ record at the resolution of the TEX_{86}-based SST record. Benthic $\delta^{18}O$ record of Site 1264 with the $\delta^{18}O$ equivalent of minimum Antarctic ice-volume estimates following Liebrand et al. (2017). These estimates are based on a constant bottom-water temperature of 2.5°C (modern-day value at Site U1364) and assume temperatures cannot drop lower. Oi-glaciation events according to Gradstein et al. (2012). Mg/Ca-based bottom-water temperatures of Site 1218 according to Lear et al. (2004) with LOESS curve average (thick black line) and 95%-confidence interval (dotted lines).

Clim. Past Discuss., https://doi.org/10.5194/cp-2017-153
Manuscript under review for journal Clim. Past
Discussion started: 14 December 2017

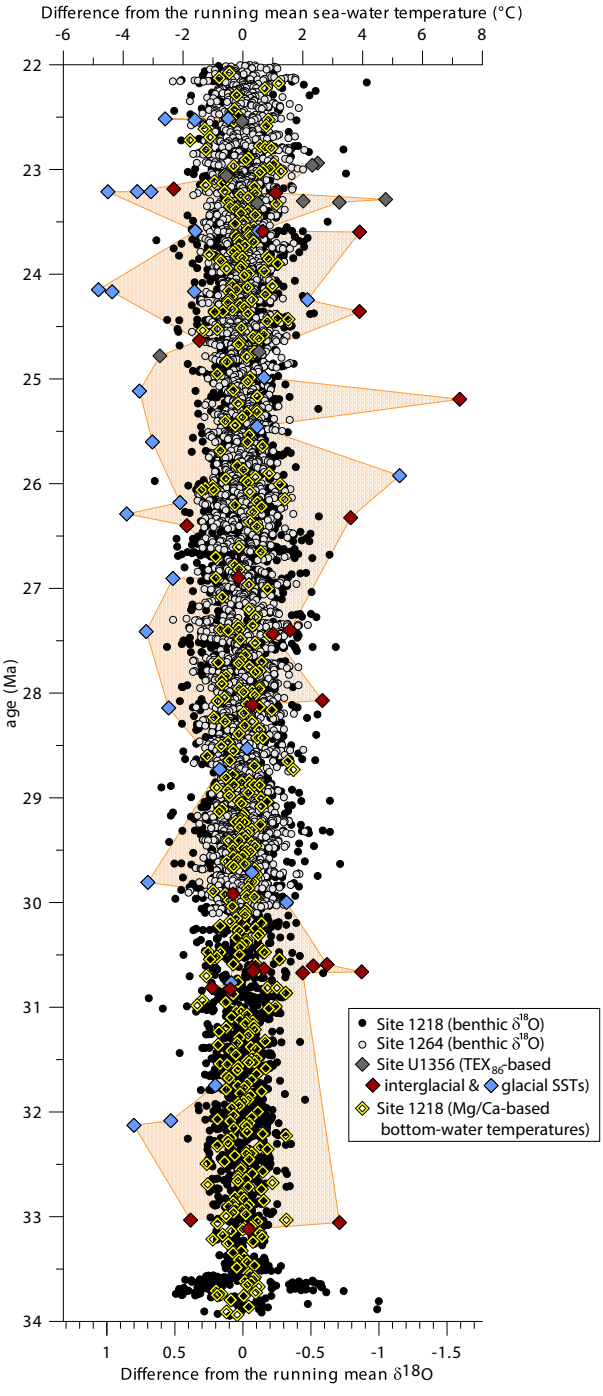

Figure 5: Comparison between the differences from our TEX_{86}-based SST mean (orange diamonds; shading indicates the range) with the differences from the benthic $\delta^{18}O$ mean from ODP Sites 1218 (Pälike et al., 2006) and 1264 (Liebrand et al., 2017, 2016) (black and grey dots), and differences from the Mg/Ca-based bottom-water temperature mean of Site 1218 (Lear et al., 2004).